ACS Chemical Neuroscience

Anatolian University Libraries Consortium a·n·k·o·s

Subscriber access provided by ORTA DOGU TEKNIK UNIVERSITESI KUTUPHANESI

Article

Targeting the Nrf2/amyloid-beta liaison in Alzheimer's disease: a rational approach

Elena Simoni, Melania M Serafini, Roberta Caporaso, Chiara Marchetti, Marco Racchi, Anna Minarini, Manuela Bartolini, Cristina Lanni, and Michela Rosini

ACS Chem. Neurosci., **Just Accepted Manuscript** • Publication Date (Web): 19 Apr 2017

Just Accepted

ACS Publications

ACS Chemical Neuroscience is published by the American Chemical Society. 1155 Sixteenth Street N.W., Washington, DC 20036

Targeting the Nrf2/amyloid-beta *liaison* in Alzheimer's disease: a rational approach

Elena Simoni,[1,ϕ] Melania M. Serafini,[2,3,ϕ] Roberta Caporaso,[1] Chiara Marchetti,[1] Marco Racchi,[2] Anna Minarini,[1] Manuela Bartolini,[1] Cristina Lanni,[2] Michela Rosini[1]*

[1]Department of Pharmacy and Biotechnology, Alma Mater Studiorum-University of Bologna, Via Belmeloro 6, 40126 Bologna, Italy

[2]Department of Drug Sciences (Pharmacology Section), V.le Taramelli 14, 27100 Pavia, Italy

[3]Scuola Universitaria Superiore IUSS Pavia, P.zza Vittoria, 15, 27100 Pavia, Italy

Keywords:

Alzheimer's disease, amyloid aggregation, Nrf2 pathway, oxidative stress, electrophilic compounds.

Abstract

Amyloid is a prominent feature of Alzheimer's disease (AD). Yet, a linear linkage between amyloid-β peptide (Aβ) and the disease onset and progression has recently been questioned. In this context, the crucial partnership between Aβ and Nrf2 pathways is acquiring paramount importance, offering prospects for deciphering the Aβ-centered disease network. Here, we report on a new class of anti-aggregating agents rationally designed to simultaneously activate transcription-based antioxidant responses, whose lead **1** showed interesting properties in a preliminary investigation. Relying on the requirements of Aβ recognition, we identified the catechol derivative **12**. In SH-SY5Y neuroblastoma cells, **12** combined remarkable free radical scavenger properties to the ability to trigger the Nrf2 pathway and induce the Nrf2-dependent defensive gene NQO1 by means of electrophilic activation of the transcriptional response. Moreover, **12** prevented the formation of cytotoxic stable oligomeric intermediates, being significantly more effective, and *per se* less toxic, than prototype **1**. More importantly, as different chemical features were exploited to regulate Nrf2 and Aβ activities, the two pathways could be tuned independently. These findings point to compound **12** and its derivatives as promising tools for investigating the therapeutic potential of the Nrf2/Aβ cellular network, laying foundation for generating new drug leads to confront AD.

INTRODUCTION

Alzheimer's disease (AD) is the most common form of neurodegenerative dementia.[1] As for major chronic diseases, its phenotype reflects several pathological processes that interact in a complex network.[2] Despite considerable efforts, the underlying disease mechanisms and their connections are still poorly understood, and it remains unclear whether they participate in neuronal degeneration with causative roles or they merely represent the telltale remains of earlier pathogenic events.

The process of amyloidogenesis is thought to be an important driver of AD. The amyloid-β peptide (Aβ) becomes harmful when Aβ monomers combine in various aggregates to form oligomers and

fibrils.[3] Aβ aggregates emerge as manifestations and mediators of a variety of neurobiological events, including inflammatory responses, tau phosphorylation impairment, mitochondrial dysfunction and oxidative damage.[4] Thus, focusing on Aβ alone has probably guided to a simplistic linear disease model, which is now appearing inadequate to represent the complexity of the disease.[5] In this context, the simultaneous observation of multiple components is increasingly being perceived as a more adequate way for addressing Aβ pluralism of causes and effects.[6-9] In this scenario, oxidative stress seems to play an important role, interconnecting diverse AD-related phenomena.[10] Indeed, the pro-oxidant environment induced by Aβ in AD pathology is a consolidated concept.[11] At the same time, oxidative stress is known to trigger the amyloidogenic pathway and promote Aβ toxicity in a vicious circle.[12] This crucial partnership involves the nuclear factor (erythroid-derived 2)-like 2 (Nrf2) transcriptional pathway, an intrinsic mechanism of defense that, under neuropathological conditions, reduces oxidative stress and inflammation by promoting the transcription of cytoprotective genes, including NAD(P)H:quinone reductase (NQO1), heme oxygenase-1 (HO-1), and glutathione S-transferase (GST) to name a few.[13, 14] The activation of this master regulator occurs by disrupting interaction and binding of Nrf2 to Kelch-like ECH-associated protein 1 (Keap 1), a cytosolic Nrf2 repressor that acts as a sensor of oxidative/electrophilic stress.[15] Notwithstanding the extensive oxidative damage characterizing AD, levels of some Nrf2-induced gene products are reduced in AD patients, suggesting disruption of the transcriptional pathway.[16] In addition, recent studies have demonstrated activation of the Keap1-Nrf2 system to be essential for counteracting Aβ-induced toxicity while genetic ablation of Nrf2 worsens amyloid deposition and neuroinflammation in a mouse model of AD.[17]

On these premises, we believe that the identification of pharmacologic tools able to modulate Aβ and/or Nrf2 pathways might contribute to the comprehension of this crucial cross-talk, offering a powerful key for interpreting the mechanistic connection between the process of protein aggregation and tissue degeneration. We have preliminary reported on a set of three molecules as

versatile tools for investigating the molecular mechanisms potentially involved in chronic Aβ damage.[18] In particular, we identified the catechol derivative **1**, which joins a remarkable anti-aggregating ability to oxidant properties. Interestingly, the biological profile of compound **1** was strategically tuned by the hydroxyl substituents on the aromatic moiety, offering a peculiar "on–off" pattern of control of the anti-aggregating efficacy that has contributed to shed light on the interconnection between the overproduction of radical species and Aβ.[18]

On this basis and in the pursuit of more effective molecules, we performed systematic modifications of **1**, by focusing on the aryl substitution pattern, the thioester function, and the aliphatic skeleton (compounds **2-13**, Figure 1).

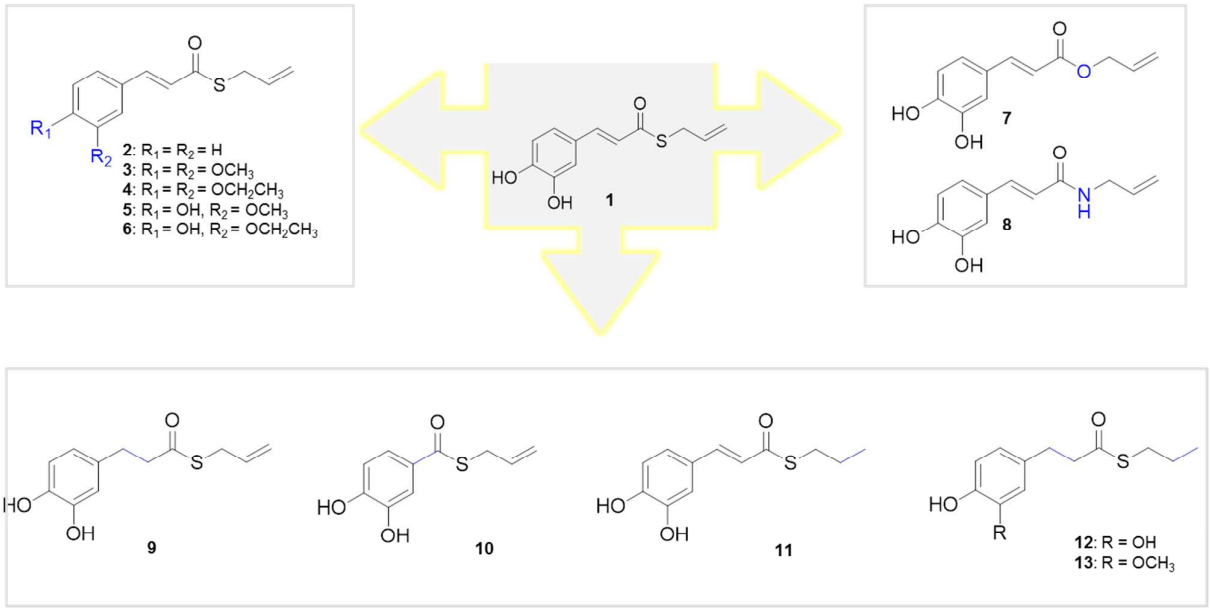

Figure 1. Drug design strategy of compounds **2-13**.

In this paper, we delineate the general structure−activity relationships (SAR) of **2**−**12** by investigating antioxidant and anti-aggregating properties. The efficacy in inhibiting fibrilization of $A\beta_{42}$, the most amyloidogenic isoform of Aβ, was first studied *in vitro* by a fluorescence-based

assay. Compounds were then assayed in human SH-SY5Y neuroblastoma cells to explore their ability to contrast oxidative stress and to exert neuroprotective effect against $A\beta_{42}$-induced toxicity. To draw connections between the structural requirements involved in inhibition of amyloid aggregation and transcription-based antioxidant responses, selected compounds were studied as Nrf2 inducers in human SH-SY5Y neuroblastoma cells, and the ability of promoting the endogenous up-regulation of the Nrf2-dependent defensive gene NQO1 was also assessed.

RESULTS AND DISCUSSION

Syntheses of the thioester derivatives **2-4** were accomplished by one pot reaction with minor modifications of literature procedure referred to caffeate esters.[19] As reported in Scheme 1 (method A), this procedure allowed Meldrum's acid mono-thioesterification with allyl sulphide to give the non-isolable intermediate, which was then readily condensed with the appropriate aldehyde affording cinnamic derivatives **2-4** with moderate to good yields.

Unfortunately, this convenient method was not effective to access the phenolic derivatives **5-13**. They were therefore synthesized by means of an alternative procedure, which minimized side-reactions and purification efforts (Scheme 1, method B). TBDMS-protected alcohols **14-19** underwent coupling reaction with the appropriate allyl or propyl derivative with DCC in presence of DMAP, to give intermediates **20-28.** Treatment of **20-28** with TBAF effected desilylation to give the final compounds **5-13**. ^{1}HNMR spectra show that compounds **2-8** and **11**, featuring a carbon-carbon double bond between the catechol ring and the carbonyl function, have an *E* configuration as indicated by the large spin coupling constants (around 16 Hz) of α-H and β-H on double bonds.

Scheme 1

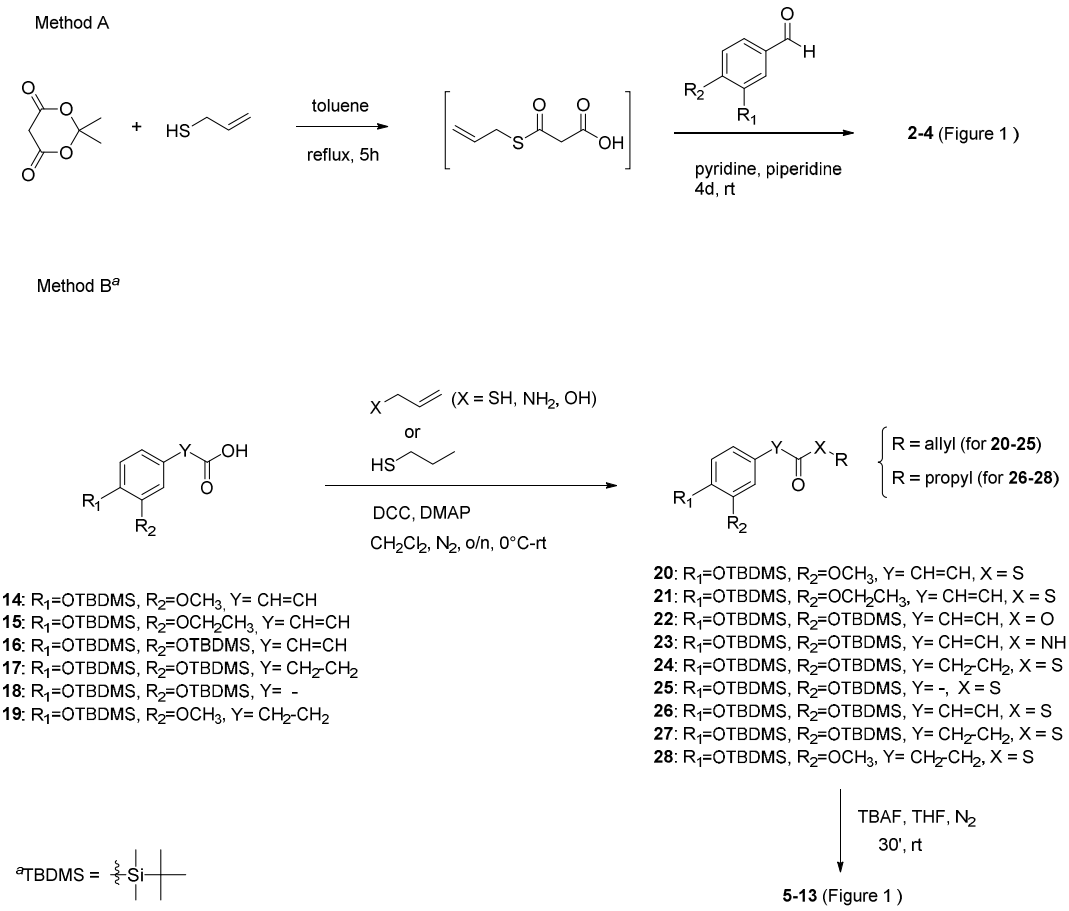

Cell toxicity assay.

In order to define the range of concentration to be used in cellular experimental settings, the cytotoxicity of compounds **2-13** was assessed in SH-SY5Y human neuroblastoma cells, in comparison with **1**. Cells were exposed to the compounds at concentrations ranging from 1 to 12.5 μM for 24 h and cell viability was evaluated by MTT assay. As shown in figure 2, all the compounds were well tolerated (reduction of cell viability of about 10%) at a concentration up to 5 μM, resulting significantly less toxic than prototype **1**, that at this concentration determined a slight decrease (about 20%) of cell viability.

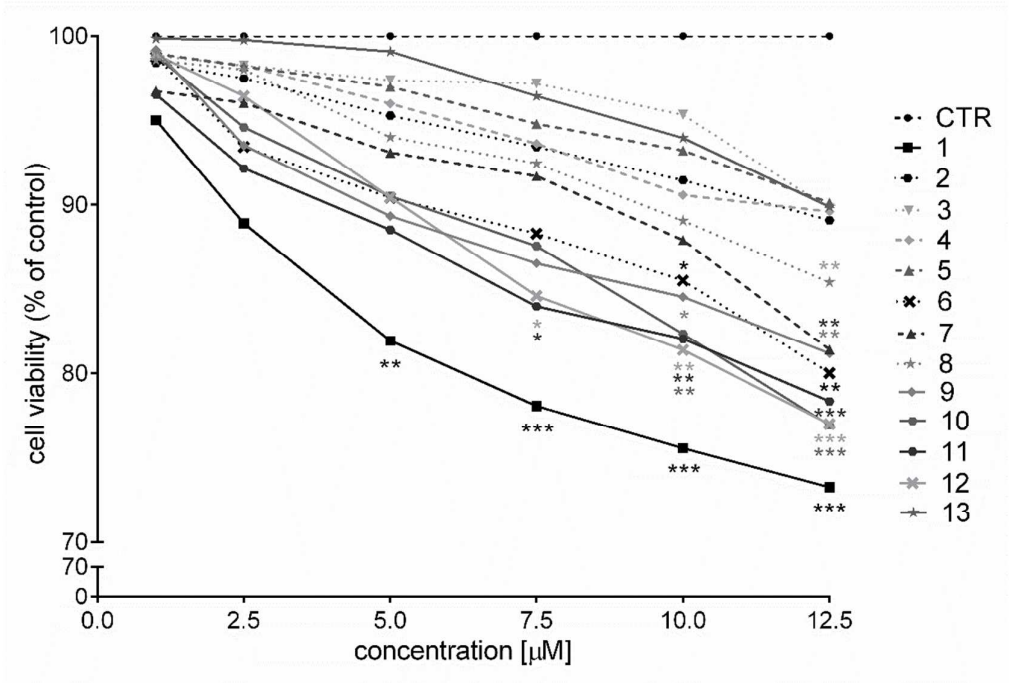

Figure 2. Cellular toxicity of compounds **2-12** on human neuroblastoma SH-SY5Y cells. The cell toxicity profiles of reference compound **1** and the non-(pro)electrophilic derivative **13** are also shown. Cells were treated with 1 μM, 2.5 μM, 5 μM, 7.5 μM, 10 μM and 12.5 μM of each compound for 24 h. Cell viability was assessed by MTT assay. Data are expressed as percentage of cell viability versus CTR; * $p<0.05$, **$p<0.01$, ***$p<0.001$ versus CTR; Dunnett's multiple comparison test.

Inhibition of $A\beta_{42}$ self-aggregation.

In our previous study, we identified catechol derivative **1** as a good inhibitor of $A\beta_{42}$ self-aggregation.[18] Its inhibitory effect was studied by a thioflavin T (ThT)-based fluorometric assay, giving an IC_{50} of 12.5 ± 0.9 μM, and confirmed by a mass spectrometry assay,[20] which allowed to detect and quantitate the monomeric form of $A\beta_{42}$. Interestingly, the anti-aggregating profile of **1** seemed to be strictly related to the catechol moiety, as a complete loss of efficacy was observed following single removal of the *m*- or *p*-hydroxyl function.

Table 1. Inhibition of $A\beta_{42}$ self-aggregation by compounds 1-12

Compd	Inhibition of $A\beta_{42}$ self-aggregation [a]	
	% inhibition (± SEM) *[I] = 50 μM*	IC_{50} μM (± SEM)
1	> 90	12.5 ± 0.9
2	< 10	nd
3	< 10	nd
4	< 10	nd
5	< 10	nd
6	< 10	nd
7	68.8 ± 7.9	34.6 ± 6.8
8	36.3 ± 7.6	nd
9	> 90	8.72 ± 0.61
10	49.1 ± 6.3	nd
11	> 90	3.99 ± 0.39
12	> 90	3.80 ± 0.44

[a] Inhibition of $A\beta_{42}$ 50 μM self-aggregation by [I] = 50 μM. The $A\beta_{42}$/inhibitor ratio was equal to 1/1. For compounds showing a % inhibition higher than 50% when screened at 50 μM the IC_{50} value was determined. Values are the mean of two independent experiments each performed in duplicate. nd stands for not determined. SEM = standard error of the mean.

Herein, systematic modifications of the aromatic substitution pattern corroborated the importance of the catechol group in inhibiting amyloid aggregation[21] as, in compounds **2**-**6**, the removal or masking into a methoxy- or ethoxy-function of one or both the hydroxyl substituents of **1** resulted in a complete loss of anti-aggregating efficacy (% inhibition at 50 μM <10%, Table 1). Following this observation, catechol-based compounds were studied to assess the role of the thioester function. Replacement of this moiety with an ester or an amide, affording compounds **7** and **8**, respectively, resulted in a gradual decrease in the ability of limiting fibril formation (-CONH-<-COO-<-COS-, Table 1). Based on these results, we can argue that the catechol motif is essential but not *per se* sufficient to guarantee anti-aggregating efficacy, indicating the thioester moiety as a second requisite of relevance in this respect. Thus, we focused on the chemical link between the above-

mentioned key features of **1**. For compound **9**, where saturation of the cinnamoyl double bond avoids conjugation of the catechol moiety and the thioester function, a slight increase in activity is observed with respect to prototype **1** (IC_{50} values equal to 8.72 and 12.5 μM for **9** and **1**, respectively), suggesting that no electronic influence between the two groups is required. Conversely, when the conjugation persists but the distance is shortened, as in **10**, a significant drop in activity is detected (from % inhibition >90 to 49.1 at 50 μM), revealing the importance of the relative position of the catechol group and the thioester side chain in amyloid recognition. Interestingly, the anti-aggregating effect of most active compounds **1** and **9** was further improved by replacing the terminal allyl moiety with an alkyl function, affording **11** (IC_{50} = 3.99 μM) and **12** (IC_{50} = 3.80 μM), respectively. This modification, in addition to potentiating prototype's efficacy, opens perspectives for further functionalization in this position as a promising multitarget drug discovery strategy.[22]

Protective effect of 12 on $A\beta_{42}$-induced toxicity in SH-SY5Y neuroblastoma cells.

Based on the promising data obtained in the in vitro assessment of the anti-aggregating properties of the new derivatives, we studied whether the most active compound **12** could also exert neuroprotective effect against $A\beta_{42}$-induced toxicity in SH-SY5Y human neuroblastoma cells. Incubation of SH-SY5Y cells with 10 μM $A\beta_{42}$ resulted in a reduction of about 40% of cell viability (as determined by MTT assay), which can be ascribed to oligomeric species formation.[23]

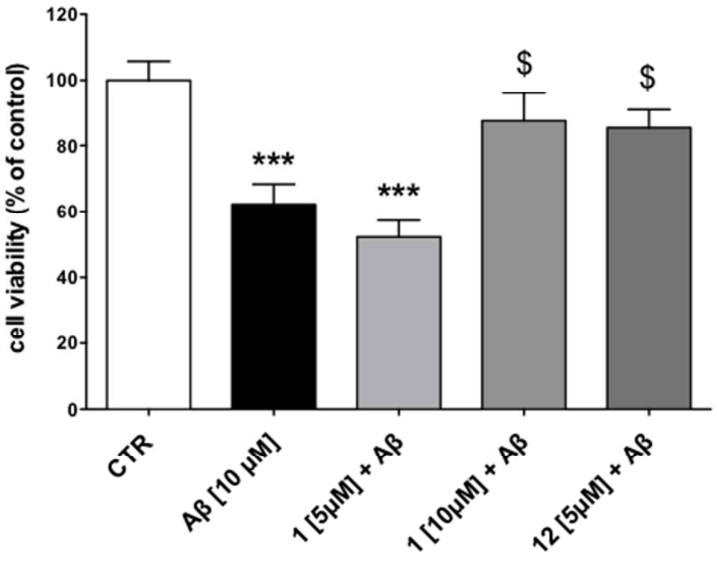

Figure 3. Effect of **1** and **12** on $A\beta_{42}$-mediated toxicity in neuroblastoma cells. SH-SY5Y cells were co-incubated for 24 h with 5 μM and 10 μM compound **1** or with 5 μM compound **12** in presence of 10 μM $A\beta_{42}$. Cell viability was determined by MTT assay. Data are expressed as percentage of cell viability versus CTR; ***$p<0.001$ versus CTR, \$ $p<0.05$ versus $A\beta_{42}$; Dunnett's multiple comparison test.

A strong protective effect was observed for compound **12** which, at 5 μM, almost completely prevented the $A\beta_{42}$-induced cell death, showing to be more effective than **1** that, in the same assay, was not able to counteract $A\beta_{42}$ toxicity up to 10 μM concentration (Figure 3). These data are in agreement with the inhibitory potency (as IC_{50} values) determined by ThT-based assay, which showed a 3.3-fold higher anti-aggregating activity for **12** compared to **1** (Table 1). A good correlation between data obtained by ThT- and cell-based assays was also previously demonstrated by others.[24]

Protective effect towards H_2O_2-induced damage.

To determine the potential interest of compounds **2-12** as antioxidants, we evaluated their scavenger ability when co-incubated with 300 μM H_2O_2, using prototype **1** as comparison.

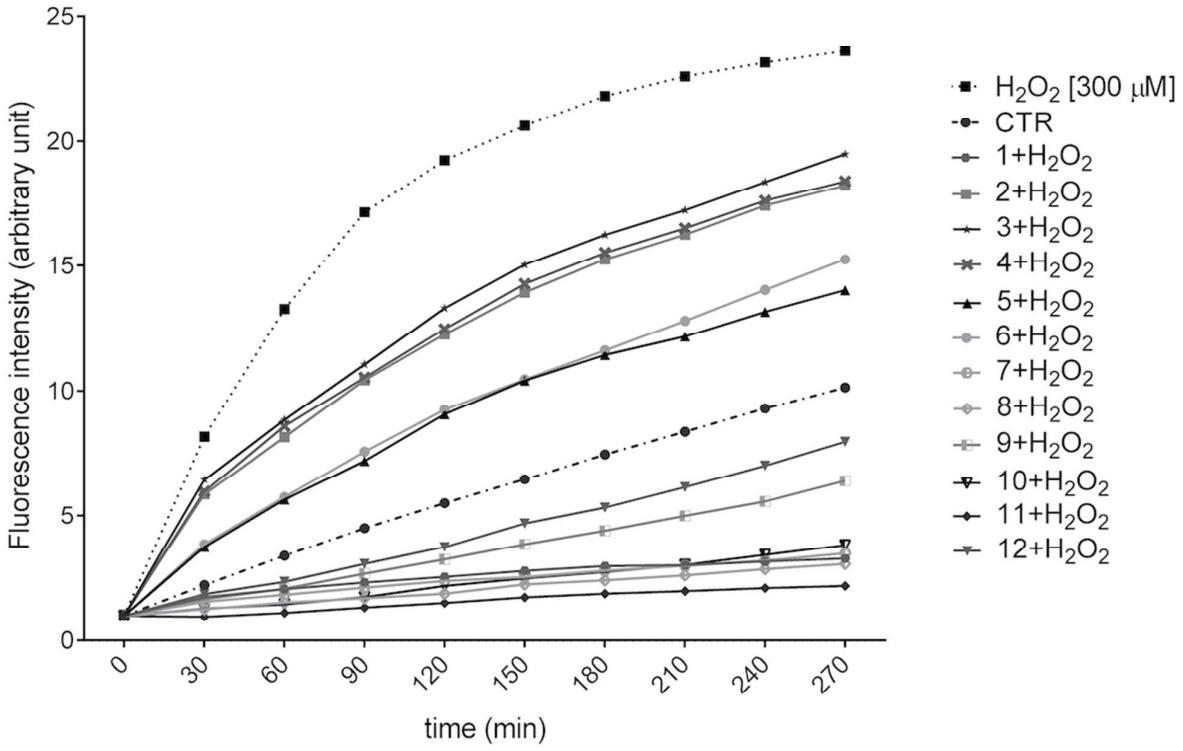

Figure 4. Compounds **1-12** reverse ROS formation induced by H_2O_2-induced oxidative stress in SH-SY5Y neuroblastoma cells. Cells were loaded with 25 mM DCFH-DA for 45 min. DCFH-DA was removed by centrifugation, cells were resuspended in PBS into a black 96-wells plate and exposed to 5 μM concentration of compounds **1-12** and 300 μM H_2O_2. ROS levels were determined from 0 to 270 min using a fluorescence microplate reader. Fluorescence intensity for all compounds is significant at any time from 30 to 270 min with $p<0.001$ versus H_2O_2. Dunnett's multiple comparison test.

ROS scavenging effects were evaluated in SH-SY5Y cells by using the fluorescent probe dichloro-dihydro-fluorescein diacetate (DCFH-DA) as a specific marker for quantitative intracellular ROS formation. In comparison to untreated cells (dashed line, Figure 4), the intracellular DCFH-fluorescence intensity in H_2O_2-treated cells significantly increased (dotted line, Figure 4). Treatment with all compounds markedly suppressed H_2O_2-induced intracellular ROS production, albeit to a different extent. In particular, catechol-based derivatives **1** and **7-12** emerged as the most potent antioxidants as, at any time tested, they were able to keep ROS levels below those observed

for control (Figure 4). This strong antioxidant activity was particularly evident for compounds where conjugation between the catechol moiety and the carbonyl function (**1**, **7**, **8**, **10** and **11**) occurs, while compounds **9** and **12**, lacking the cinnamoyl double bond, were slightly less effective.

Activation of Nrf2 pathway in neuroblastoma cells.

Activation of the Keap1/Nrf2 pathway and the consequent induction of phase 2 antioxidant genes trigger an elaborate network of protective mechanisms against oxidative damage.[25] When exposed to oxidative insults, Keap1 undergoes conformational changes as a result of oxidation at specific cysteine residues. This disrupts Nrf2 binding, promotes Nrf2 translocation into the nucleus and the activation of transcription-mediated protective responses.[26, 27] Interestingly, the Keap1-Nrf2 interaction can also be disrupted by small molecules,[28] most of which have electrophilic properties.[29] Thus, the opportunity for tuning the inducible antioxidant response is offered by Keap1 cysteine residues, which covalently conjugate the electrophilic inducers.[30] Based on these observations, electrophiles and proelectrophiles from synthetic or natural sources have attracted interest from a broad range of researchers in the drug discovery community.[31] In particular, proelectrophile compounds, which include hydroquinone cores of terpenoids and flavonoids, are only converted to their active electrophilic forms in response to pathological oxidation, offering prospects of minimal potential side effects.[32]

Herein, based on the (pro)electrophilic features of compounds **2-12**, we selected a number of catechol-based derivatives to be studied as Nrf2 inducers. First, by acting as the "on" switch for anti-aggregating activity, the catechol group represented a prerequisite for exploring the amyloid/Nrf2 cellular network. Secondly, catechols, which become active *ortho*-quinones on oxidation, prospect benefits of proelectrophiles, which should provide neuroprotection in oxidative conditions.[33] In addition, catechol-bearing compounds **1** and **7-12** can count on more favorable

scavenger abilities (as highlighted by their ability to reverse H_2O_2-induced ROS formation), which can significantly contribute to the overall antioxidant profile of the new molecules.

Thus, catechol derivatives **1** and **7-12** were investigated in SH-SY5Y neuroblastoma cell line to verify whether they may affect the Nrf2 pathway. To note, some of the selected compounds also presented an electrophilic α,β-unsaturated carbonyl group (Michael acceptor functionality), which may represent an additional source for Nrf2 activation. To discriminate the individual contribution of the two (pro)electrophilic features, compound **5**, where the Michael acceptor is not associated to the catechol moiety, and a new compound (**13**) lacking both electrophilic functionalities (purposely synthesized) were tested for comparison. Nrf2 protein levels were evaluated by western immunoblotting in SH-SY5Y cells after treatment for 24 h with compounds **1**, **5** and **7-13** at 5 μM concentration. Interestingly, all compounds with the exception of **13** increased Nrf2 levels when compared to control (Fig. 5a), suggesting that Nrf2 modulation can be driven by both the catechol function and the α,β-unsaturated carbonyl group, while the other structural features seemed to have modest relevance in this respect. In particular, differently from what observed for the anti-aggregating activity, the thioester group is not a key feature for inducing Nrf2 activation, as demonstrated by the strong efficacy elicited by ester derivative **7**. The lack of efficacy observed for compound **13** suggests that nucleophilic addition of Keap1 cysteine residues to (pro)electrophilic portions of the molecule may represent the initiating event of the transcriptional process. Thus, we focused on the activation of Nrf-2 signalling by analyzing its translocation into nucleus and its ability to induce NQO1, a prototypical cytoprotective Nrf2-target gene related to cellular stress response. In particular, we selected compounds **1**, **5**, **7**, **9** and **12**, which increased significantly the protein levels of Nrf2. The selected compounds carry alternatively or simultaneously the two (pro)electrophilic features responsible for Nrf2 induction. Compound **13** was also tested as negative control. All compounds, with the only exception of **13**, induced remarkable Nrf2 nuclear translocation, with catechol derivatives **1**, **7**, **9** and **12** being slightly more effective than **5**, lacking

the catechol moiety (Figure 5b). Moreover, when analyzing the induction of NQO1, all the compounds but **13** increased NQO1 levels, with the same trend of activity detected for Nrf2 activation and translocation to the nucleus (Figure 5c). Noteworthy, differently from what recently observed for other multi-electrophile compounds,[34] the combined presence of the two (pro)electrophilic features, as in **1**, did not result in a synergistic efficacy (compare activity of **1** with that of **9** and **12**, which only carry the catechol group). This can be possibly ascribed to the conjugation, occurring in **1**, between the two features, that consequently may not behave as separate entities.

a

Total Nrf2 protein expression levels										
	CTR	**1**	**5**	**7**	**8**	**9**	**10**	**11**	**12**	**13**
Nrf2/ tubulin	100,0	411,3	339,9	383,1	188,0	372,3	198,7	231,5	367,3	138,7
SEM	7,835	42,60	43,64	28,51	21,18	58,03	28,04	15,89	63,32	14,44
P-value	/	< 0,0001	< 0,0001	< 0,0001	0,5640	0,0002	0,4378	0,1617	< 0,0001	0,9813

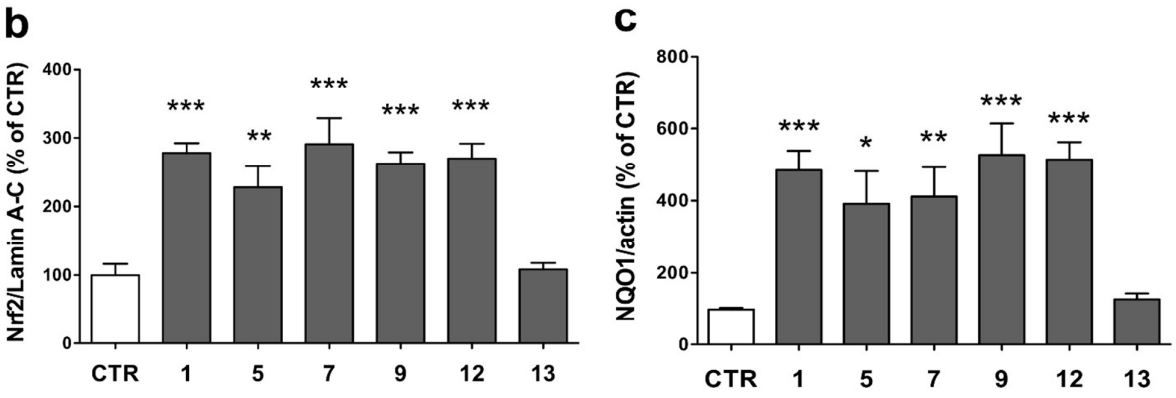

Figure 5. Activation of Nrf2-mediated phase II detoxification pathway**. a)** Total cellular extracts of SH-SY5Y cells treated for 24 h with 5 μM concentration of compounds **1**, **5**, **7**-**13** were analyzed for Nrf2 expression by western blot. Anti tubulin was used as protein loading control. Results are shown as ratio Nrf2/tubulin (% of CTR) ± SEM. Dunnett's multiple comparison test. **b)** Nuclear cellular extracts of SH-SY5Y cells were treated for 3 h with compounds **1**, **5**, **7**, **9**, **12**, **13** at 5 μM concentration and homogenized to obtain nuclear fraction. Nrf2 expression was determined by western blot. Anti lamin A-C was used as protein

loading control. Results are shown as ratio Nrf2/lamin A-C (% of CTR) ± SEM. **p<0.01 and ***p<0.001 versus CTR; Dunnett's multiple comparison test. **c)** Total cellular extracts of SH-SY5Y cells treated for 24 h with 5 μM concentration of compounds **1**, **5**, **7**, **9**, **12**, **13** were analyzed for NQO1 expression by western blot. Anti-actin was used as protein loading control. Results are shown as ratio NQO1/actin (% of CTR) ± SEM. *p<0.05, **p<0.01 and ***p<0.001 versus CTR; Dunnett's multiple comparison test.

Electrophilic features may account for potential toxicity issues associated with off-target interactions.[34] When studied in SH-SY5Y cells the non-(pro)electrophilic compound **13** was not toxic in the whole range of tested concentrations (cell viability > 90%, Figure 2). Noteworthy, the behavior at 5 μM (concentration of interest for biological activity) of (pro)electrophilic compounds **2-12** was not significantly dissimilar from that of **13**.

Conclusion

Advances in Aβ-centered drug discovery for AD suffer the lack of a molecular mechanistic theory of Aβ causative role. Thus, a deeper comprehension of the intertwined correlation between Aβ and oxidative damage might contribute to the understanding and treatment of the disease. The interest towards this critical partnership is reinforced by the emerging evidence of an aberrant regulation of the Nrf2-mediated antioxidant response in AD, with Aβ contributing to the dysfunctional activation of the transcriptional pathway.

On these bases, in the pursuit of more effective anti-aggregating and antioxidant properties, we herein expanded our previous study on the catechol derivative **1** through systematic modifications of its structure. We also deepened insight the antioxidant profile of the compounds by investigating their ability to trigger the Nrf2 pathway in terms of up-regulation of Nrf2 expression, translocation into the nucleus and induction of the Nrf2-dependent defensive gene NQO1. Interestingly, in SH-SY5Y neuroblastoma cells, all compounds tested exhibited remarkable free radical scavenging

properties and protected against oxidative stress by means of electrophilic activation of Nrf2-mediated response. This multimodal behavior was accompanied by a significant reduction of the cytotoxicity with respect to **1**. Relying on the requirements of Aβ recognition, which was driven by the catechol function and the thioester group, we identified compound **12**. It joined the above-mentioned antioxidant effects to a marked ability of preventing the formation of cytotoxic stable oligomeric intermediates, being significantly more effective than prototype **1**. Most importantly, as different chemical features were exploited to regulate Nrf2 and Aβ activities, we could finely and separately tune the two pathways. These findings point to compound **12** and its derivatives as powerful tools for investigating the therapeutic potential of the Nrf2/Aβ cellular network, paving the way for the generation of new drug leads to confront AD.

EXPERIMENTAL SECTION

Chemistry. ***General Chemical methods.*** Chemical reagents were purchased from Sigma Aldrich, Fluka and Lancaster (Italy). The course of the reactions was observed by TLC on 0.20 mm silica gel 60 F254 plates (Merck, Germany), then visualized with an UV lamp. Nuclear magnetic resonance spectra (NMR) were recorded at 400 MHz for ^{1}H and 100 MHz for ^{13}C on Varian VXR 400 spectrometer. Chemical shifts are reported in parts per millions (ppm) relative to tetramethylsilane (TMS), and spin multiplicities are given as s (singlet), br s (broad singlet), d (doublet), t (triplet), q (quartet), or m (multiplet). Direct infusion ESI-MS mass spectra were recorded on a Waters ZQ 4000 apparatus. Final compounds **1**−**13** were >95% pure as determined by HPLC analyses. The analyses were performed under reversed-phase conditions on a Phenomenex Jupiter C18 (150x4.6 mm I.D.) column, using a binary mixture of H_2O/acetonitrile (60/40, v/v for **2**, **5**, **6**; 30/70, v/v for **3**,**4**; 65/35, v/v for **7**, **10**, **11**; 70/30, v/v for **8**; 50/50, v/v for **9**, **12**, **13**) as the mobile phase, UV detection at λ = 302 nm (for **2**-**8**, **10**) or 254 nm (for **9**, **12**, **13**) and a flow rate of 0.7 mL/min.

Analyses were performed on a liquid chromatograph model PU-1585 UV equipped with a 20 μL loop valve (Jasco Europe, Italy).

General procedure for the target compounds 2-4. To a solution of Meldrum's acid (1 equiv, 114.13 mg, 4.05 mmol) in toluene (8 mL) was slowly added 2-propene-1-thiol (1 equiv, 300 mg, 4.05 mmol). The mixture was refluxed for 7 h. After the formation of the intermediate, the reaction was cooled to room temperature followed by sequential addition of the appropriate aldehyde (0.4 equiv), pyridine (400 μL) and piperidine (40 μL). The stirring continued at room temperature 4 days. Following evaporation of the solvent, the residue was purified by column chromatography on silica gel to yield the desired cinnamic derivatives **2-4**.

***S*-allyl (*E*)-3-phenylprop-2-enethioate (2). 2** was synthesized from benzaldehyde (170 mg, 1.6 mmol). Elution with petroleum ether/ethyl acetate (9.7:0.3) afforded **2** as a waxy solid: 108 mg (33%). ^{1}H NMR (400 MHz, $CDCl_3$) δ 7.58 (d, *J*=15.6 Hz, 1H), 7.47-7.44 (m, 2H), 7.32-7.29 (m, 3H), 6.67 (d, *J*=15.6 Hz, 1H), 5.89-5.79 (m, 1H), 5.26 (dd, ^{1}J=16.8 Hz, ^{2}J=1.2 Hz, 1H), 5.10 (d, *J*=10 Hz, 1H), 3.64 (d, *J*=6.8 Hz, 2H). ^{13}C NMR (100 MHz, $CDCl_3$) δ 190.04, 140.63, 134.06, 133.19, 130.58, 128.94 (2 C), 128.43 (2 C), 124.75, 117.99, 31.80. MS [ESI^+] *m/z* 227 $[M+Na]^+$.

***S*-allyl (*E*)-3-(3,4-dimethoxyphenyl)prop-2-enethioate (3). 3** was synthesized from 3,4-dimethoxybenzaldehyde (266 mg, 1.6 mmol). Elution with petroleum ether/ethyl acetate (7:3) afforded **3** as a white solid: 220 mg (52%), m.p.= 123 °C. ^{1}H NMR (400 MHz, $CDCl_3$) δ 7.57 (d, *J*=16 Hz, 1H), 7.13 (dd, ^{1}J=8 Hz, ^{2}J=2 Hz, 1H), 7.05 (d, *J*=2Hz, 1H), 6.86 (d, *J*=8 Hz, 1H), 6.59 (d, *J*=16 Hz, 1H), 5.91-5.84 (m, 1H), 5.29 (d, *J*=19.6, 1H), 5.13 (d, *J*=11.6, 1H), 3.92 (s, 6H), 3.67 (d, *J*=8 Hz, 2H). ^{13}C-NMR (100 MHz, $CDCl_3$) δ 188.88, 151.44, 149.25, 140.77, 133.21, 126.95, 123.26, 122.58, 117.86, 111.04, 109.74, 55.98 (2 C), 31.71. MS [ESI^+] *m/z* 265 $[M+1]^+$.

***S*-allyl (*E*)-3-(3,4-diethoxyphenyl)prop-2-enethioate (4). 4** was synthesized from 3,4-diethoxybenzaldehyde (310 mg, 1.6 mmol). Cristallization from ethanol gave **4** as a white solid: 220 mg (47%), m.p. =145 °C; ^{1}H NMR (400 MHz, $CDCl_3$) δ 7.53 (d, *J*=15.6 Hz, 1H), 7.09-7.05

(m, 2H), 6.83 (d, *J*=8 Hz, 1H), 6.57 (d, *J*=15.6 Hz, 1H), 5.89-5.83 (m, 1H), 5.27 (d, *J*=17.2 Hz, 1H), 5.11 (d, *J*=10.4 Hz, 1H), 4.13-4.08 (m, 4H), 3.66 (d, *J*=6.8 Hz, 2H), 1.47-1.44 (m, 6H). ^{13}C-NMR (100 MHz, $CDCl_3$) δ 188.76, 151.28, 148.79, 140.90, 133.27, 126.75, 123.21, 122.36, 117.78, 112.63, 112.0, 64.58 (2 C), 31.67, 14.74 (2 C). MS [ESI^+] *m/z* 315 $[M+Na]^+$.

General procedure for the intermediates 14-19. To a solution of the appropriate commercially available acid (1 equiv) in dry DMF (5 mL) were added TBDMS-Cl (2-3 equiv) and imidazole (5 equiv) under nitrogen atmosphere. After leaving the reaction to room temperature overnight, the mixture was concentrated to dryness, and the residue purified by column chromatography on silica gel to yield the desired intermediates **14-19**. Experimental data of known compounds **14** and **16-19** were in agreement with the literature.

(*E*)-3-(4-((*tert*-butyldimethylsilyl)oxy)-3-ethoxyphenyl)acrylic acid (15). 15 was synthesized from (*E*)-3-(3-ethoxy-4-hydroxyphenyl)acrylic acid (500 mg, 2.40 mmol). Elution with petroleum ether/ethyl acetate/methanol (5:4.5:0.5) afforded **15** as a waxy solid: 325 mg (42%); ^{1}H NMR (400 MHz, $CDCl_3$) δ 7.70 (d, *J*=15.6 Hz, 1H), 7.03 (s, 1H), 7.02 (d, *J*=4.0 Hz, 1H), 6.84 (d, *J*=4.0 Hz, 1H), 6.30 (d, *J*=15.6 Hz, 1H), 4.04 (q, *J*=7.2 Hz, 2H), 1.45 (t, *J*=6.8 Hz, 3H), 0.99 (s, 9H), 0.17 (s, 6H). ^{13}C NMR (100 MHz, $CDCl_3$) 171.57, 152.21, 148.89, 147.65, 126.62, 122.91, 121.31, 114.01, 111.09, 64.93, 31.76, 25.61 (3 C), 14.73, -4.61 (2 C).

General procedure for the intermediates 20-28. To an ice-cooled solution of the appropriate protected acid (**14-19**) (1 equiv) in dry CH_2Cl_2 (4 mL) was added DCC (1.1 equiv), and DMAP (cat.). The reaction mixture was stirred for 10 min, followed by addition of the appropriate nucleophile (3 equiv). Stirring was then continued at room temperature overnight, and the reaction worked up by filtration and evaporation. The crude was purified by chromatography on silica gel.

***S*-allyl (*E*)-3-(4-((*tert*-butyldimethylsilyl)oxy)-3-methoxyphenyl)prop-2-enethioate (20). 20** was synthesized from **14**[35] (410 mg, 1.33 mmol) and 2-propene-1-thiol. Elution with petroleum ether/ethyl acetate (9.4:0.6) afforded **20** as a waxy solid: 330 mg (68%); ^{1}H NMR (400 MHz, $CDCl_3$) δ 7.48 (d, *J*=15.6 Hz, 1H), 6.98-6.95 (m, 2H), 6.76 (d, *J*=8 Hz, 1H), 6.50 (d, *J*=15.6 Hz,

1H), 5.80-5.76 (m, 1H), 5.21 (d, *J*=18 Hz, 1H), 5.05 (d, *J*=10 Hz, 1H), 3.76 (s, 3H), 3.59 (d, *J*=6.80 Hz, 2H), 0.91 (s, 9H), 0.09 (s, 6H). ^{13}C NMR (100 MHz, $CDCl_3$) 174.87, 151.23, 147.94, 140.97, 133.25, 127.84, 122.81, 122.66, 121.14, 117.84, 111.00, 55.44, 31.70, 25.63 (3 C), 18.46, -4.61 (2 C).

***S*-allyl (*E*)-3-(4-((*tert*-butyldimethylsilyl)oxy)-3-ethoxyphenyl)prop-2-enethioate (21). 21** was synthesized from **15** (200 mg, 0.62 mmol) and 2-propene-1-thiol. Elution with petroleum ether/ethyl acetate (9.5:0.5) afforded **21** as a waxy solid: 130 mg (55%); ^{1}H NMR (400 MHz, $CDCl_3$) δ 7.50 (d, *J*=16 Hz, 1H), 7.00-6.89 (m, 2H), 6.79 (d, *J*=8 Hz, 1H), 6.52 (d, *J*=16 Hz, 1H), 5.86-5.77 (m, 1H), 5.22 (d, *J*=17.2 Hz, 1H), 5.10 (d, *J*=10 Hz, 1H), 4.01 (q, *J*=6.4 Hz, 2H), 3.62 (d, *J*=6.8 Hz, 2H), 1.41 (t, *J*=6.4 Hz, 3H), 0.96 (s, 9H), 0.03 (s, 6H). ^{13}C NMR (100 MHz, $CDCl_3$) δ 189.04, 146.34, 145.99, 140.85, 132.27, 125.39, 124.69, 122.15, 117.64, 114.96, 111.02, 64.93, 31.90, 24.93 (3 C), 18.66, 14.35, -4.31 (2 C).

Allyl (*E*)-3-(3,4-bis((*tert*-butyldimethylsilyl)oxy)phenyl)acrylate (22). 22 was synthesized from **16**[35] (190 mg, 0.465 mmol) and allyl alcohol. Elution with petroleum ether/ethyl acetate (9.5:0.5) afforded **22** as a waxy solid: 120 mg (57%); ^{1}H NMR (400 MHz, $CDCl_3$) δ 7.57 (d, *J*=16 Hz, 1H), 6.99 (s, 1H), 6.98 (d, *J*=8 Hz, 1H) 6.80 (d, *J*=8 Hz, 1H) 6.23 (d, *J*=16 Hz, 1H), 6.00-5.98 (m, 1H), 5.34 (d, *J*=16 Hz, 1H), 5.24 (d, *J*=11 Hz, 1H), 4.67 (d, *J*=6 Hz, 2H), 0.97 (s, 9H), 0.96 (s, 9H), 0.19 (s, 6H), 0.18 (s, 6H). ^{13}C NMR (100 MHz, $CDCl_3$) δ 169.8, 146.93, 146.04, 143.71, 133.03, 126.06, 122.03, 118.64, 115.29, 114.85, 114.00, 30.07, 26.63 (6 C), 18.56 (2 C), -4.21 (4 C).

(*E*)-*N*-allyl-3-(3,4-bis((*tert*-butyldimethylsilyl)oxy)phenyl)acrylamide (23). 23 was synthesized from **16**[35] (400 mg, 0.978 mmol) and allylamine. Elution with petroleum ether/ethyl acetate (8:2) afforded **23** as a waxy solid: 100 mg (23%); ^{1}H NMR (400 MHz, $CDCl_3$) δ 7.49 (d, *J*=15.6 Hz, 1H), 6.98 (s, 1H), 6.96 (d, *J*=8 Hz, 1H), 6.77 (d, *J*=8 Hz, 1H), 6.21 (d, *J*=15.6 Hz, 1H), 5.91-5.80 (m, 1H), 5.81 (br s, 1H), 5.21 (d, *J*=17.2 Hz, 1H), 5.13 (d, *J*=11.6 Hz, 1H), 3.99 (d, *J*=5.6 Hz, 2H), 0.97 (s, 9H), 0.96 (s, 9H), 0.19 (s, 6H), 0.18 (s, 6H). ^{13}C NMR (100 MHz, $CDCl_3$) δ 166.95, 147.31,

145.20, 141.17, 133.93, 127.02, 121.55, 117.63, 115.34, 114.80, 113.52, 41.20, 25.63 (6 C), 18.76 (2 C), -4.11 (4 C).

***S*-allyl 3-(3,4-bis((*tert*-butyldimethylsilyl)oxy)phenyl)propanethioate (24). 24** was synthesized from **17**[36] (300 mg, 0.73 mmol) and 2-propene-1-thiol. Elution with petroleum ether/ethyl acetate (9.7:0.3) afforded **24** as a waxy solid: 200 mg (59%); ^{1}H NMR (400 MHz, $CDCl_3$) δ 6.71(d, *J*=8 Hz, 1H), 6.62-6.57 (m, 2H), 5.78-5.73 (m, 1H), 5.20 (dd, ^{1}J=16.8 Hz, ^{2}J=1.2 Hz, 1H), 5.07 (d, *J*=8 Hz, 1H), 3.51 (d, *J*=8 Hz, 2H), 2.84-2.77 (m, 4H), 0.97 (s, 18H), 0.17 (s, 12H). ^{13}C-NMR (100 MHz, $CDCl_3$) δ 198.09, 146.78 (2 C), 145.42, 133.22, 121.34, 121.24, 121.10, 117.99, 45.79, 31.09, 30.86, 26.09 (6 C), 18.57 (2 C), -3.96 (4 C).

***S*-allyl 3,4-bis((*tert*-butyldimethylsilyl)oxy)benzothioate (25). 25** was synthesized from **18**[37] (330 mg, 0.862 mmol) and 2-propene-1-thiol. Elution with petroleum ether/ethyl acetate (8:2) afforded **25** as a waxy solid: 130 mg (34%); ^{1}H NMR (400 MHz, $CDCl_3$) δ 7.51-7.47 (m, 2H), 6.84 (d, *J*=8 Hz, 1H), 5.88 (m, 1H), 5.30 (d, *J*=17.2 Hz, 1H), 5.13 (d, *J*=10 Hz, 1H), 3.69 (d, *J*=6.8 Hz, 2H), 0.99 (s, 18H), 0.22 (s, 12H). ^{13}C NMR (100 MHz, $CDCl_3$) δ 190.30, 151.34, 146.49, 134.01, 130.94, 120.42, 117.82, 115.96, 114.76, 32.28, 25.72 (6 C), 18.57 (2 C), -4.06 (4 C).

***S*-propyl (*E*)-3-(3,4-bis((*tert*-butyldimethylsilyl)oxy)phenyl)prop-2-enethioate (26). 26** was synthesized from **16**[35] (480 mg, 1.174 mmol) and 1-propanethiol. Elution with petroleum ether/ethyl acetate (9.8:0.2) afforded **26** as a waxy solid: 430 mg (78%); ^{1}H NMR (400 MHz, $CDCl_3$) δ 7.49 (d, *J*=16 Hz, 1H), 7.05-7.01 (m, 2H), 6.82 (d, *J*=8.4 Hz, 1H), 6.52 (d, *J*=16 Hz, 1H), 2.99 (t, *J*=7.2 Hz, 2H), 1.70-1.64 (m, 2H), 1.03-0.97 (m, 18H + 3H), 0.21 (s, 12H). ^{13}C NMR (100 MHz, $CDCl_3$) δ 190.70, 145.84, 144.52, 141.95, 126.95, 122.98, 121.65, 115.54, 114.83, 32.14, 24.08, 25.52 (6 C), 18.53 (2 C), 13.32, -4.16 (4 C).

***S*-propyl 3-(3,4-bis((*tert*-butyldimethylsilyl)oxy)phenyl)propanethioate (27). 27** was synthesized from **17**[36] (300 mg, 0.73 mmol) and 1-propanethiol. Elution with petroleum ether/ethyl acetate (9.7:0.3) afforded **27** as a waxy solid: 342 mg (44%); ^{1}H NMR (400 MHz, $CDCl_3$) δ 6.72 (d, *J*= 8 Hz, 1H), 6.64 (s, 1H), 6.61 (d, *J*=8 Hz, 1H), 2.86-2.79 (m, 6H), 1.60-1.55 (m, 2H), 0.99-0.93 (m,

18H+3H), 0.18 (s, 12H). ^{13}C NMR (100 MHz, $CDCl_3$) δ 198.86, 146.74, 145.35, 133.35, 121.33, 121.25, 121.06, 45.91, 30.94, 30.87, 26.07 (6 C), 23.07, 18.54 (2 C), 13.45, -3.98 (4 C).

***S*-propyl 3-(4-((*tert*-butyldimethylsilyl)oxy)-3-methoxyphenyl)propanethioate (28). 28** was synthesized from **19**[38] (110 mg, 0.35mmol) and 1-propanethiol. Elution with petroleum ether/ethyl acetate (9.5:0.5) afforded **28** as a pale oil: 70 mg (54%); ^{1}H NMR (400MHz, $CDCl_3$) δ 6.75 (d, *J*=8 Hz, 1H), 6.67 (d, *J*=2 Hz, 1H), 6.63 (dd,^{1}*J*=8 Hz,^{2}*J*=2 Hz, 1H), 3.78 (s, 3H), 2.91-2.86 (m, 2H), 2.85-2.82 (m, 4H), 1.62-1.56 (m, 2H), 0.99 (s, 9H), 0.97-0.94 (m, 3H), 0.14 (s, 6H).^{13}C NMR (100MHz, $CDCl_3$) δ 198.96, 150.90, 143.55, 143.55, 133.69, 120.90, 112.54, 55.57, 45.95, 31.38, 30.88, 25.83 (3 C), 23.06, 18.53, 13.39, -4.56 (2 C).

General procedure for the synthesis of 5-13. To a solution of the appropriate organosilane intermediate **20-28** (1 equiv) in THF (5 mL) was added TBAF (4 equiv) and stirring was continued at room temperature. After 20-30 min, the reaction was quenched by addition of saturated aqueous NH_4Cl solution; the aqueous phase was extracted with EtOAc (3 x 10 mL), and the combined organic layer was dried over Na_2SO_4. Following evaporation of the solvent, the residue was purified by column chromatography on silica gel.

***S*-allyl (*E*)-3-(4-hydroxy-3-methoxyphenyl)prop-2-enethioate (5). 5** was synthesized from **20** (330 mg, 0.91mmol). Elution with petroleum ether/ethyl acetate (8.5:1.5) afforded **5** as a waxy solid: 140 mg (62%); ^{1}H NMR (400 MHz, $CDCl_3$) δ 7.54 (d, *J*=15.6 Hz, 1H), 7.08 (d, *J*=8 Hz, 1H), 7.01 (s, 1H), 6.90 (d, *J*=8 Hz, 1H), 6.56 (d, *J*=15.6 Hz, 1H), 5.90 (br s, 1H), 5.87-5.80 (m, 1H), 5.27 (d, *J*=16.8 Hz, 1H), 5.11 (d, *J*=10 Hz, 1H), 3.92 (s, 3H), 3.65 (d, *J*=7.6 Hz, 2H). ^{13}C NMR (100 MHz, $CDCl_3$) δ 188.91, 148.31, 146.79, 140.95, 133.23, 126.57, 123.66, 122.35, 117.86, 114.81, 109.49, 55.98, 31.71. MS [ESI$^-$] m/z 249 $[M-1]^-$.

***S*-allyl (*E*)-3-(3-ethoxy-4-hydroxyphenyl)prop-2-enethioate (6). 6** was synthesized from **21** (120 mg, 0.317 mmol). Elution with petroleum ether/ethyl acetate (8.5:1.5) afforded **6** as a waxy solid: 50 mg (60%); ^{1}H NMR (400 MHz, $CDCl_3$) δ 7.52 (d, *J*=15.6 Hz, 1H), 7.06 (d, *J*=8 Hz, 1H), 6.99 (s, 1H), 6.90 (d, *J*=8 Hz, 1H), 6.54 (d, *J*=15.6 Hz, 1H), 5.90 (br s, 1H), 5.89-5.84 (m, 1H), 5.26 (d,

J=16.8 Hz, 1H), 5.10 (d, *J*=9.6 Hz, 1H), 4.13 (q, *J*=7.2 Hz, 2H), 3.64 (d, *J*=7.2 Hz, 2H), 1.45 (t, *J*=7.2 Hz, 3H). ^{13}C NMR (100 MHz, $CDCl_3$) δ 188.94, 148.44, 146.09, 141.05, 133.25, 126.49, 123.49, 122.25, 117.84, 114.76, 110.42, 64.63, 31.70, 14.75. MS [ESI$^+$] *m/z* 265 $[M+1]^+$; [ESI$^-$] *m/z* 263 $[M-1]^-$.

Allyl (*E*)-3-(3,4-dihydroxyphenyl)acrylate (7).[19] **7** was synthesized from **22** (120 mg, 0.267 mmol). Elution with petroleum ether/ethyl acetate (5:5) afforded **7** as a waxy solid: 43 mg (73%); ^{1}H NMR (400 MHz, $CDCl_3$) δ 7.59 (d, *J*=16 Hz, 1H), 7.09 (s, 1H), 6.98 (d, *J*=8 Hz, 1H), 6.86 (d, *J*=8 Hz, 1H), 6.26 (d, *J*=16 Hz, 1H), 5.97-5.93 (m, 1H), 5.35(d, *J*=17.2 Hz, 1H), 5.26(d, *J*=10.4 Hz, 1H), 4.70 (d, *J*=5.6 Hz, 2H). ^{13}C NMR (100 MHz, $CDCl_3$) δ 167.8, 146.63, 145.65, 143.91, 132.03, 127.26, 122.53, 118.44, 115.49, 114.97, 114.40, 29.67. MS [ESI$^+$] *m/z* 221 $[M+1]^+$; [ESI$^-$] *m/z* 219 $[M-1]^-$.

(*E*)-*N*-allyl-3-(3,4-dihydroxyphenyl)acrylamide (8).[39] **8** was synthesized from **23** (100 mg, 0.224 mmol). Elution with $CHCl_3$/MeOH (9.7:0.3) afforded **8** as a waxy solid: 40 mg (81%);^{1}H NMR (400 MHz, CD_3OD) δ 7.39 (d, *J*=15.6 Hz, 1H), 6.99 (s, 1H), 6.89 (d, *J*=8 Hz, 1H), 6.74 (d, *J*=8 Hz, 1H), 6.37 (d, *J*=15.6 Hz, 1H), 5.91-5.82 (m, 1H), 5.18(d, *J*=17.2 Hz, 1H), 5.11 (d, *J*=13.2 Hz, 1H), 3.89 (d, *J*=7.2 Hz, 2H). ^{13}C NMR (100 MHz, CD_3OD) δ 167.75, 147.41, 145.30, 141.14, 134.03, 126.82, 120.75, 116.63, 115.04, 114.90, 113.68, 41.50. MS [ESI$^+$] *m/z* 220 $[M+1]^+$; [ESI$^-$] *m/z* 218 $[M-1]^-$.

***S*-allyl 3-(3,4-dihydroxyphenyl)propanethioate (9). 9** was synthesized from **24** (130 mg, 0.28 mmol). Elution with petroleum ether/ethyl acetate (5.5:4.5) afforded **9** as a waxy oil: 45 mg (67%); ^{1}H NMR (400 MHz, $CDCl_3$) δ 6.77 (d, *J*=8 Hz, 1H), 6.69 (s, 1H), 6.61 (d, *J*=8 Hz, 1H), 5.84-5.73 (m, 1H), 5.22 (d, *J*=17.2 Hz, 1H), 5.10 (d, *J*=10.8 Hz, 1H), 3.53 (d, *J*=7.2 Hz, 2H), 2.89-2.80 (m, 4H). ^{13}C NMR (100 MHz, $CDCl_3$) δ 199.25, 143.71, 142.18, 132.95 (2 C), 120.77, 118.18, 115.56, 115.50, 45.68, 31.96, 30.91. MS [ESI$^+$] *m/z* 261 $[M+Na]^+$.

***S*-allyl 3,4-dihydroxybenzothioate (10). 10** was synthesized from **25** (130 mg, 0.296 mmol). Elution with dichloromethane/methanol (9.8:0.2) afforded **10** as a dark oil: 15 mg (20%); ^{1}H NMR (400 MHz, CD_3OD) δ 7.41-7.38 (m, 2H), 6.81 (d, *J*=8.4 Hz, 1H), 5.91-5.82 (m, 1H), 5.27 (d, *J*=16.8 Hz, 1H), 5.09 (d, *J*=9.6 Hz, 1H), 3.66 (d, *J*=6.8 Hz, 2H). ^{13}C NMR (100 MHz, CD_3OD) δ 191.30, 152.35, 146.49, 135.01, 130.24, 121.53, 117.92, 115.92, 114.96, 32.38. MS [ESI^+] *m/z* 209 $[M+1]^+$.

S-propyl (*E*)-3-(3,4-dihydroxyphenyl)prop-2-enethioate (11). 11 was synthesized from **26** (430 mg, 0.921 mmol). Elution with dichloromethane/methanol (9.6:0.4) afforded **11** as a pale oil: 63 mg (30%); ^{1}H NMR (400 MHz, $CDCl_3$) δ 7.50 (d, *J*=15.6 Hz, 1H), 7.10 (s, 1H), 7.02 (d, *J*=8 Hz, 1H), 6.88 (d, *J*=8 Hz, 1H), 6.56 (d, *J*=15.6 Hz, 1H), 2.98 (t, *J*=7.2 Hz, 2H), 1.69-1.64 (m, 2H), 1.00 (t, *J*=7.2 Hz, 3H). ^{13}C NMR (100 MHz, $CDCl_3$) δ 191.80, 146.88, 144.02, 140.92, 127.25, 122.98 (2 C), 115.74, 114.93, 31.13, 23.08, 13.52. MS [ESI^-] *m/z* 237 $[M-1]^-$.

***S*-propyl 3-(3,4-dihydroxyphenyl)propanethioate (12). 12** was synthesized from **27** (119 mg, 0.25 mmol). Elution with petroleum ether/ethyl acetate (5.5:4.5) afforded **12** as a waxy oil: 41 mg (66%); ^{1}H NMR (400 MHz, $CDCl_3$) δ 6.76 (d, *J*=8.4 Hz, 1H), 6.68 (d, *J*=2 Hz 1H),6.59 (dd, ^{1}*J*=8.4, ^{2}*J*=2 Hz 1H), 2.86-2.81 (m, 6H), 1.58-1.57 (m, 2H), 0.94 (t, *J*=7.2 Hz, 3H). ^{13}C NMR (100 MHz, $CDCl_3$) δ 200.23, 143.60, 142.07, 132.89, 120.61, 115.44, 115.39, 45.71, 30.92, 30.88, 22.82, 13.27. MS [ESI^+] *m/z* 263 $[M+Na]^+$.

***S*-propyl 3-(4-hydroxy-3-methoxyphenyl)propanethioate (13). 13** was synthesized from **28** (70 mg, 0.189 mmol). Elution with petroleum ether/ethyl acetate (5.5:4.5) afforded **13** as a pale oil: 45 mg (94%); ^{1}H NMR (400 MHz, $CDCl_3$) δ 6.83-6.81 (m, 1H), 6.68 (s, 1H), 6.66 (d, *J*=2 Hz, 1 H), 3.86 (s, 3H), 2.92-2.80 (m, 6H), 1.61-1.56 (m, 2 H), 0.95 (t, *J*=8 Hz, 3H). ^{13}C NMR (100 MHz, $CDCl_3$) δ 199.14, 146.62, 144.23, 132.25, 121.10, 114.56, 111.14, 56.07, 46.15, 31,47, 30.10, 23.16, 13.51. MS [ESI^+] *(m/z)* 277 $[M+Na]^+$.

Sample preparation for $A\beta_{42}$ self-aggregation.

1,1,1,3,3,3-Hexafluoro-2-propanol (HFIP)-pretreated $A\beta_{42}$ samples (Bachem AG, Switzerland) were resolubilized with a CH_3CN/0.3 mM Na_2CO_3/250 mM NaOH (48.4:48.4:3.2) mixture to have a stable stock solution ([$A\beta_{42}$]=500 μM).[20, 40] Tested inhibitors were dissolved in MeOH and diluted in the assay buffer. Experiments were performed by incubating the peptide diluted in 10 mM phosphate buffer (pH 8.0) containing 10 mM NaCl at 30°C (Thermomixer Comfort, Eppendorf, Italy) for 24 h (final Aβ concentration=50 μM) with and without inhibitor.

Inhibition of $A\beta_{42}$ self-aggregation: ThT assay. Inhibition studies were performed by incubating $A\beta_{42}$ samples in the assay conditions reported above, with and without tested inhibitors. Inhibitors were first screened at 50 μM in a 1:1 ratio with $A\beta_{42}$. To quantify amyloid fibril formation, the ThT fluorescence method was used.[41] After incubation, samples were diluted to a final volume of 2.0 mL with 50 mM glycine-NaOH buffer (pH = 8.5) containing 1.5 μM ThT. A 300-seconds-time scan of fluorescence intensity was carried out (λ_{exc} = 446 nm; λ_{em} = 490 nm), and values at plateau were averaged after subtracting the background fluorescence of 1.5 μM ThT solution. Blanks containing inhibitor and ThT were also prepared and evaluated to account for quenching and fluorescence properties. The fluorescence intensities were compared and the % inhibition was calculated. For compounds **7**, **9**, **11** and **12**, the IC_{50} value was also determined. To this aim four increasing concentrations were tested. IC_{50} value was obtained from the % inhibition *vs* log[inhibitor] plot.

Reagents for cellular experiments. All culture media, supplements and Foetal Bovine Serum (FBS) were obtained from Euroclone (Life Science Division, Milan, Italy). Electrophoresis reagents were obtained from Bio-Rad (Hercules, CA, USA). All other reagents were of the highest grade available and were purchased from Merck KGaA (Darmstadt, Germany) unless otherwise indicated. $A\beta_{42}$ was solubilized in dimethyl sulfoxide (DMSO) at the concentration of 100 μM and frozen in stock aliquots. All the experiments performed with Aβ were made in 1% of serum. H_2O_2 was diluted to working concentration (300 μM) in phosphate buffer saline (PBS) at the moment of use.

Cell cultures. Human neuroblastoma SH-SY5Y cell line from European Collection of Cell Cultures (ECACC No. 94030304) were cultured in medium with equal amount of Eagle's minimum essential medium and Nutrient Mixture Ham's F-12, supplemented with 10% foetal bovine serum, glutamine (2mM), penicillin/streptomycin, non-essential aminoacids at 37 °C in 5% CO_2/95% air.

Cell viability. The mitochondrial dehydrogenase activity that reduces 3-(4,5-dimethylthiazol-2-yl)-2,5-diphenyl-tetrazolium bromide (MTT, Sigma, St Louis, MO, USA) was used to determine cellular viability, in a quantitative colorimetric assay. At day 0 SH-SY5Y cells were plated at a density of $2.5x10^4$ viable cells per well in 96-well plates. After treatment, according to the experimental setting, cells were exposed to an MTT solution in PBS (1 mg/mL). Following 4 h incubation with MTT and treatment with SDS for 24 h, cell viability reduction was quantified by using a Synergy HT multi-detection microplate reader (Bio-Tek).

Measurement of intracellular ROS. DCFH-DA (Merck KGaA, Darmstadt, Germany) was used to estimate intracellular ROS. Two different experimental settings were performed. First, cells were loaded with 25 μM DCFH-DA for 45 min. After centrifugation DCFH-DA was removed and cells were exposed to 5 μM of compounds **1-13** and 300 μM H_2O_2. Alternatively, cells (2×10^4 cells/well) were pretreated to compounds **1-13** (5 μM) for 24 h and then loaded with 25 μM DCFH-DA at 37°C for 45 min. DCFH-DA was removed after centrifuge and cells were resuspended in PBS and then exposed to 300 μM H_2O_2. The results were visualized using Synergy HT multi-detection microplate reader (BioTek) with excitation and emission wavelengths of 485 nm and 530 nm, respectively.

Immunodetection of Nrf2 and NQO-1. Cell monolayers were washed twice with ice cold PBS, lysed on the tissue culture dish by addition of ice-cold lysis buffer (50 mM Tris/HCl pH 7.4, 150 mM NaCl, 50 mM EDTA, 0.2 mM 4-(2-aminoethyl) benzenesulfonyl fluoride hydrochloride (AEBSF), 20 μg/mL leupeptin, 25 μg/mL aprotinin, 0,5 μg/mL pepstatin A and 1% Triton X-100) and an aliquot was used for protein analysis with the Bradford assay, for protein quantification. Cell lysates were diluited in sample buffer (62.5 mM Tris/HCl pH 6.8, 2% SDS, 10% glycerol, 50 mM

dithiothreitol, 0.1% Bromophenol blue) and subjected to Western blot analysis. Proteins were subjected to SDS-PAGE (10%) and then transferred onto PVDF membrane 0,45 μm (Merck KGaA Darmstadt, Germany). The membrane was blocked for 1 h with 5% BSA in Tris-buffered saline containing 0.1% Tween 20 (TBST). Membranes were immunoblotted with the rabbit anti human Nrf2 polyclonal antibody (at 1:2000 in 5% BSA) and the mouse anti-NQO-1 monoclonal antibody (1:1000 in 5% BSA) (Novus, Bio-techne Minneapolis, USA). The detection was carried out by incubation with horseradish peroxidase conjugated goat anti-rabbit IgG for Nrf-2 or rabbit anti-mouse for NQO-1 (1:5000 dilution in 5% BSA, from Merck KGaA Darmstadt, Germany) for 1 h. The blots were then washed extensively and the proteins of interest were visualized using an enhanced chemiluminescent method (Pierce, Rockford, IL, USA). Tubulin was also performed as a normal control of proteins (Merck KGaA Darmstadt, Germany).

Subcellular fractionation for Nrf2 nuclear translocation. 5×10^6 SH-SY5Y cells were seeded in 100mm^2 dishes and treated for 3 h with 5 μM compounds **1**, **5**, **7**, **9**, **11**, **13**; afterwards the medium was removed, and cells were washed twice with ice-cold PBS. Cells were subsequently homogenized 15 times using a glass-glass dounce homogenizer in 0.32 M sucrose buffered with 20 mM Tris-HCl (pH 7.4) containing 2 mM EDTA, 0,5 mM EGTA, 50 mM β-mercaptoethanol, and 20μg/mL leupeptin, apotrinin and pepstatin. The homogenate was centrifuged at 300×g for 5 min to obtain the nuclear fraction. An aliquot of the nuclear fraction was used for protein assay by the Bradford method, whereas the remaining was boiled for 5 min after dilution with sample buffer and subjected to polyacrylamide gel electrophoresis and immunoblotting as described.

Densitometry and statistics. All the experiments, unless specified, were performed at least three times. Following acquisition of the Western blot image through an AGFA scanner and analysis by means of the Image 1.47 program (Wayne Rasband, NIH, Research Services Branch, NIMH, Bethesda, MD, USA), the relative densities of the bands were expressed as arbitrary units and normalized to data obtained from control sample run under the same conditions. Data were

analyzed by analysis of variance (ANOVA) followed when significant by an appropriate post hoc comparison test as indicated in figure legend. The reported data are expressed as means ± SEM of at least three independent experiments. A p value < 0.05 was considered statistically significant.

AUTHOR INFORMATION

$^{\phi}$ The authors contributed equally to the work.

Corresponding Author

* Michela Rosini: michela.rosini@unibo.it, Phone/Fax: +39 051 2099722/34.

Author Contributions

M.R., C.L., E.S. participated in research design; M.R., C.L., M.B. and E.S. analysed results and wrote the manuscript with input from all coauthors; M.R., C.L., M.B., A.M., M.R., E.S. conceived the methodology, designed experiments and analysed data. E.S., R.C. and C.M. afforded synthesis and characterization of compounds; M.B. ran experiments on amyloid aggregation; M.M.S. performed cellular experiments.

Funding Sources

This work was supported by the University of Bologna (grants from the RFO).

Notes

The authors declare no competing financial interest.

ABBREVIATIONS

AD, Alzheimer's disease; Aβ, amyloid-β peptide; ANOVA, analysis of variance; DCFH-DA, dichlorodihydrofluorescein diacetate; DCC, *N*,*N*'-dicyclohexylcarbodiimide; DMAP, 4-dimethylaminopyridine; DMF, *N*,*N*-dimethylformamide; DMSO, dimethyl sulfoxide; ESI-MS, electrospray ionisation mass spectrometry; FBS, Foetal Bovine Serum, GST, glutathione S-transferase; HPLC, high performance liquid chromatography; HO-1, heme oxygenase-1; Keap 1, Kelch-like ECH-associated protein 1; MTT, 3-(4,5-dimethylthiazol-2-yl)-2,5-diphenyl-tetrazolium bromide; NMR, nuclear magnetic resonance; NQO1, NAD(P)H:quinone reductase; Nrf2, nuclear factor (erythroid-derived 2)-like 2; PBS, phosphate buffer saline; ppm, parts per millions; SAR, structure-activity relationships; TBDMS, *tert*-butyldimethylsilyl; TBAF, tetrabutylammonium fluoride; TBDMS-Cl, *tert*-butyldimethylsilyl chloride; TBST, Tris-buffered saline containing 0.1% Tween 20; THF, tetrahydrofuran; TLC, thin layer chromatography; TMS, tetramethylsilane; ThT, thioflavin T; UV, ultraviolet.

References

1. Winblad, B., Amouyel, P., Andrieu, S., Ballard, C., Brayne, C., Brodaty, H., Cedazo-Minguez, A., Dubois, B., Edvardsson, D., Feldman, H., Fratiglioni, L., Frisoni, G. B., Gauthier, S., Georges, J., Graff, C., Iqbal, K., Jessen, F., Johansson, G., Jönsson, L., Kivipelto, M., Knapp, M., Mangialasche, F., Melis, R., Nordberg, A., Rikkert, M. O., Qiu, C., Sakmar, T. P., Scheltens, P., Schneider, L. S., Sperling, R., Tjernberg, L. O., Waldemar, G., Wimo, A., and Zetterberg, H. (2016) Defeating Alzheimer's disease and other dementias: a priority for European science and society. *Lancet Neurol. 15*, 455-532.
2. Iqbal, K., and Grundke-Iqbal, I. (2010) Alzheimer's disease, a multifactorial disorder seeking multitherapies. *Alzheimers Dement. 6*, 420-424.
3. Reiman, E. M. (2016) Alzheimer's disease: Attack on amyloid-β protein. *Nature 537*, 36-37.
4. Kuruva, C. S., and Reddy, P. H. (2017) Amyloid beta modulators and neuroprotection in Alzheimer's disease: a critical appraisal. *Drug Discov. Today 22*, 223-233.
5. Herrup, K. (2015) The case for rejecting the amyloid cascade hypothesis. *Nat. Neurosci. 18*, 794-799.
6. Rosini, M., Simoni, E., Bartolini, M., Soriano, E., Marco-Contelles, J., Andrisano, V., Monti, B., Windisch, M., Hutter-Paier, B., McClymont, D. W., Mellor, I. R., and Bolognesi, M. L. (2013) The bivalent ligand approach as a tool for improving the in vitro anti-Alzheimer multitarget profile of dimebon. *ChemMedChem 8*, 1276-1281.
7. Viayna, E., Sola, I., Bartolini, M., De Simone, A., Tapia-Rojas, C., Serrano, F. G., Sabaté, R., Juárez-Jiménez, J., Pérez, B., Luque, F. J., Andrisano, V., Clos, M. V., Inestrosa, N. C., and Muñoz-Torrero, D. (2014) Synthesis and multitarget biological profiling of a novel family of rhein derivatives as disease-modifying anti-Alzheimer agents. *J. Med. Chem. 57*, 2549-2567.
8. Prati, F., De Simone, A., Bisignano, P., Armirotti, A., Summa, M., Pizzirani, D., Scarpelli, R., Perez, D. I., Andrisano, V., Perez-Castillo, A., Monti, B., Massenzio, F., Polito, L., Racchi, M., Favia, A. D., Bottegoni, G., Martinez, A., Bolognesi, M. L., and Cavalli, A. (2015) Multitarget drug discovery for Alzheimer's disease: triazinones as BACE-1 and GSK-3β inhibitors. *Angew. Chem. Int. Ed. Engl. 54*, 1578-1582.
9. Minarini, A., Milelli, A., Tumiatti, V., Rosini, M., Simoni, E., Bolognesi, M. L., Andrisano, V., Bartolini, M., Motori, E., Angeloni, C., and Hrelia, S. (2012) Cystamine-tacrine dimer: a new multi-target-directed ligand as potential therapeutic agent for Alzheimer's disease treatment. *Neuropharmacology 62*, 997-1003.
10. Rosini, M., Simoni, E., Milelli, A., Minarini, A., and Melchiorre, C. (2014) Oxidative stress in Alzheimer's disease: are we connecting the dots? *J. Med. Chem. 57*, 2821-2831.
11. Butterfield, D. A., Swomley, A. M., and Sultana, R. (2013) Amyloid β-peptide (1-42)-induced oxidative stress in Alzheimer disease: importance in disease pathogenesis and progression. *Antioxid. Redox. Signal. 19*, 823-835.
12. Swomley, A. M., Förster, S., Keeney, J. T., Triplett, J., Zhang, Z., Sultana, R., and Butterfield, D. A. (2014) Abeta, oxidative stress in Alzheimer disease: evidence based on proteomics studies. *Biochim. Biophy. Acta 1842*, 1248-1257.
13. Wilson, A. J., Kerns, J. K., Callahan, J. F., and Moody, C. J. (2013) Keap calm, and carry on covalently. *J. Med. Chem. 56*, 7463-7476.
14. Itoh, K., Chiba, T., Takahashi, S., Ishii, T., Igarashi, K., Katoh, Y., Oyake, T., Hayashi, N., Satoh, K., Hatayama, I., Yamamoto, M., and Nabeshima, Y. (1997) An Nrf2/small Maf heterodimer mediates the induction of phase II detoxifying enzyme genes through antioxidant response elements. *Biochem. Biophys. Res. Commun. 236*, 313-322.
15. Lu, M. C., Ji, J. A., Jiang, Z. Y., and You, Q. D. (2016) The Keap1-Nrf2-ARE Pathway As a Potential Preventive and Therapeutic Target: An Update. *Med. Res. Rev. 36*, 924-963.

16. Ramsey, C. P., Glass, C. A., Montgomery, M. B., Lindl, K. A., Ritson, G. P., Chia, L. A., Hamilton, R. L., Chu, C. T., and Jordan-Sciutto, K. L. (2007) Expression of Nrf2 in neurodegenerative diseases. *J. Neuropathol. Exp. Neurol. 66*, 75-85.
17. Joshi, G., Gan, K. A., Johnson, D. A., and Johnson, J. A. (2015) Increased Alzheimer's disease-like pathology in the APP/ PS1ΔE9 mouse model lacking Nrf2 through modulation of autophagy. *Neurobiol. Aging 36*, 664-679.
18. Simoni, E., Serafini, M. M., Bartolini, M., Caporaso, R., Pinto, A., Necchi, D., Fiori, J., Andrisano, V., Minarini, A., Lanni, C., and Rosini, M. (2016) Nature-Inspired Multifunctional Ligands: Focusing on Amyloid-Based Molecular Mechanisms of Alzheimer's Disease. *ChemMedChem 11*, 1309-1317.
19. Xia, C. N., Li, H. B., Liu, F., and Hu, W. X. (2008) Synthesis of trans-caffeate analogues and their bioactivities against HIV-1 integrase and cancer cell lines. *Bioorg. Med. Chem. Lett. 18*, 6553-6557.
20. Bartolini, M., Naldi, M., Fiori, J., Valle, F., Biscarini, F., Nicolau, D. V., and Andrisano, V. (2011) Kinetic characterization of amyloid-beta 1-42 aggregation with a multimethodological approach. *Anal. Biochem. 414*, 215-225.
21. Simoni, E., Caporaso, R., Bergamini, C., Fiori, J., Fato, R., Miszta, P., Filipek, S., Caraci, F., Giuffrida, M. L., Andrisano, V., Minarini, A., Bartolini, M., and Rosini, M. (2016) Polyamine Conjugation as a Promising Strategy To Target Amyloid Aggregation in the Framework of Alzheimer's Disease. *ACS Med. Chem. Lett. 7*, 1145-1150.
22. Rosini, M., Simoni, E., Caporaso, R., and Minarini, A. (2016) Multitarget strategies in Alzheimer's disease: benefits and challenges on the road to therapeutics. *Future Med. Chem. 8*, 697-711.
23. Sabella, S., Quaglia, M., Lanni, C., Racchi, M., Govoni, S., Caccialanza, G., Calligaro, A., Bellotti, V., and De Lorenzi, E. (2004) Capillary electrophoresis studies on the aggregation process of beta-amyloid 1-42 and 1-40 peptides. *Electrophoresis 25*, 3186-3194.
24. Pouplana, S., Espargaro, A., Galdeano, C., Viayna, E., Sola, I., Ventura, S., Muñoz-Torrero, D., and Sabate, R. (2014) Thioflavin-S staining of bacterial inclusion bodies for the fast, simple, and inexpensive screening of amyloid aggregation inhibitors. *Curr. Med. Chem. 21*, 1152-1159.
25. Baird, L., and Dinkova-Kostova, A. T. (2011) The cytoprotective role of the Keap1-Nrf2 pathway. *Arch. Toxicol. 85*, 241-272.
26. Suzuki, T., and Yamamoto, M. (2015) Molecular basis of the Keap1-Nrf2 system. *Free Radic Biol Med 88*, 93-100.
27. Abed, D. A., Goldstein, M., Albanyan, H., Jin, H., and Hu, L. (2015) Discovery of direct inhibitors of Keap1-Nrf2 protein-protein interaction as potential therapeutic and preventive agents. *Acta Pharm. Sin. B 5*, 285-299.
28. Jiang, Z. Y., Lu, M. C., and You, Q. D. (2016) Discovery and Development of Kelch-like ECH-Associated Protein 1. Nuclear Factor Erythroid 2-Related Factor 2 (KEAP1:NRF2) Protein-Protein Interaction Inhibitors: Achievements, Challenges, and Future Directions. *J. Med. Chem. 59*, 10837-10858.
29. Magesh, S., Chen, Y., and Hu, L. (2012) Small molecule modulators of Keap1-Nrf2-ARE pathway as potential preventive and therapeutic agents. *Med. Res. Rev. 32*, 687-726.
30. Kobayashi, M., and Yamamoto, M. (2006) Nrf2-Keap1 regulation of cellular defense mechanisms against electrophiles and reactive oxygen species. *Adv. Enzyme Regul. 46*, 113-140.
31. Satoh, T., Stalder, R., McKercher, S. R., Williamson, R. E., Roth, G. P., and Lipton, S. A. (2015) Nrf2 and HSF-1 Pathway Activation via Hydroquinone-Based Proelectrophilic Small Molecules is Regulated by Electrochemical Oxidation Potential. *ASN Neuro. 7*.
32. Satoh, T., McKercher, S. R., and Lipton, S. A. (2014) Reprint of: Nrf2/ARE-mediated antioxidant actions of pro-electrophilic drugs. *Free Radic. Biol. Med. 66*, 45-57.

33. Lipton, S. A., Rezaie, T., Nutter, A., Lopez, K. M., Parker, J., Kosaka, K., Satoh, T., McKercher, S. R., Masliah, E., and Nakanishi, N. (2016) Therapeutic advantage of pro-electrophilic drugs to activate the Nrf2/ARE pathway in Alzheimer's disease models. *Cell Death Dis. 7*, e2499.
34. Deny, L. J., Traboulsi, H., Cantin, A. M., Marsault, É., Richter, M. V., and Bélanger, G. (2016) Bis-Michael Acceptors as Novel Probes to Study the Keap1/Nrf2/ARE Pathway. *J. Med. Chem. 59*, 9431-9442.
35. Rattanangkool, E., Kittikhunnatham, P., Damsud, T., Wacharasindhu, S., and Phuwapraisirisan, P. (2013) Quercitylcinnamates, a new series of antidiabetic bioconjugates possessing α-glucosidase inhibition and antioxidant. *Eur. J. Med. Chem. 66*, 296-304.
36. Allegretta, G., Weidel, E., Empting, M., and Hartmann, R. W. (2015) Catechol-based substrates of chalcone synthase as a scaffold for novel inhibitors of PqsD. *Eur. J. Med. Chem. 90*, 351-359.
37. Cervellati, R., Galletti, P., Greco, E., Cocuzza, C. E., Musumeci, R., Bardini, L., Paolucci, F., Pori, M., Soldati, R., and Giacomini, D. (2013) Monocyclic β-lactams as antibacterial agents: facing antioxidant activity of N-methylthio-azetidinones. *Eur. J. Med. Chem. 60*, 340-349.
38. Toneto Novaes, L. F., Martins Avila, C., Pelizzaro-Rocha, K. J., Vendramini-Costa, D. B., Pereira Dias, M., Barbosa Trivella, D. B., Ernesto de Carvalho, J., Ferreira-Halder, C. V., and Pilli, R. A. (2015) (-)-Tarchonanthuslactone: Design of New Analogues, Evaluation of their Antiproliferative Activity on Cancer Cell Lines, and Preliminary Mechanistic Studies. *ChemMedChem 10*, 1687-1699.
39. Rajan, P., Vedernikova, I., Cos, P., Berghe, D. V., Augustyns, K., and Haemers, A. (2001) Synthesis and evaluation of caffeic acid amides as antioxidants. *Bioorg. Med. Chem. Lett. 11*, 215-217.
40. Bartolini, M., Bertucci, C., Bolognesi, M. L., Cavalli, A., Melchiorre, C., and Andrisano, V. (2007) Insight into the kinetic of amyloid beta (1-42) peptide self-aggregation: elucidation of inhibitors' mechanism of action. *ChemBioChem 8*, 2152-2161.
41. Naiki, H., Higuchi, K., Hosokawa, M., and Takeda, T. (1989) Fluorometric determination of amyloid fibrils in vitro using the fluorescent dye, thioflavin T1. *Anal. Biochem. 177*, 244-249.

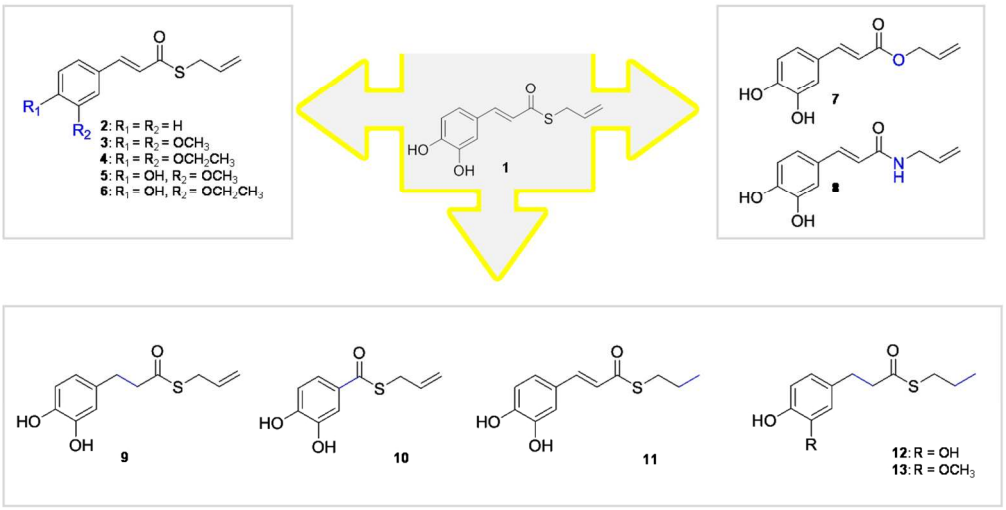

Figure 1. Drug design strategy of compounds 2-13.

116x73mm (300 x 300 DPI)

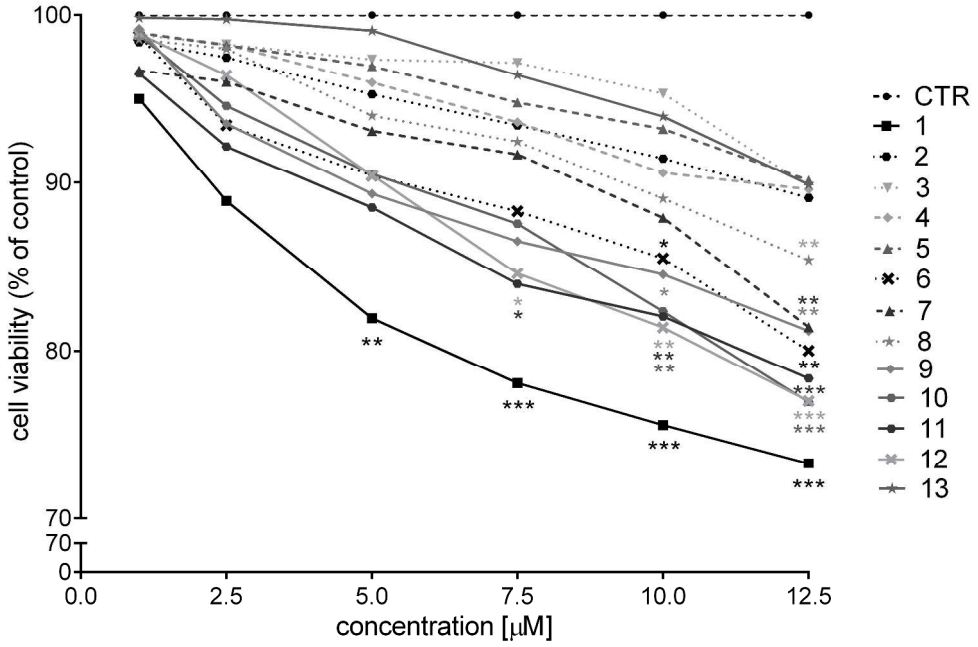

Figure 2. Cellular toxicity of compounds 2-12 on human neuroblastoma SH-SY5Y cells. The cell toxicity profiles of reference compound 1 and the non-(pro)electrophilic derivative 13 are also shown. Cells were treated with 1 μM, 2.5 μM, 5 μM, 7.5 μM, 10 μM and 12.5 μM of each compound for 24 h. Cell viability was assessed by MTT assay. Data are expressed as percentage of cell viability versus CTR; * $p<0.05$, ** $p<0.01$, *** $p<0.001$ versus CTR; Dunnett's multiple comparison test.

414x282mm (300 x 300 DPI)

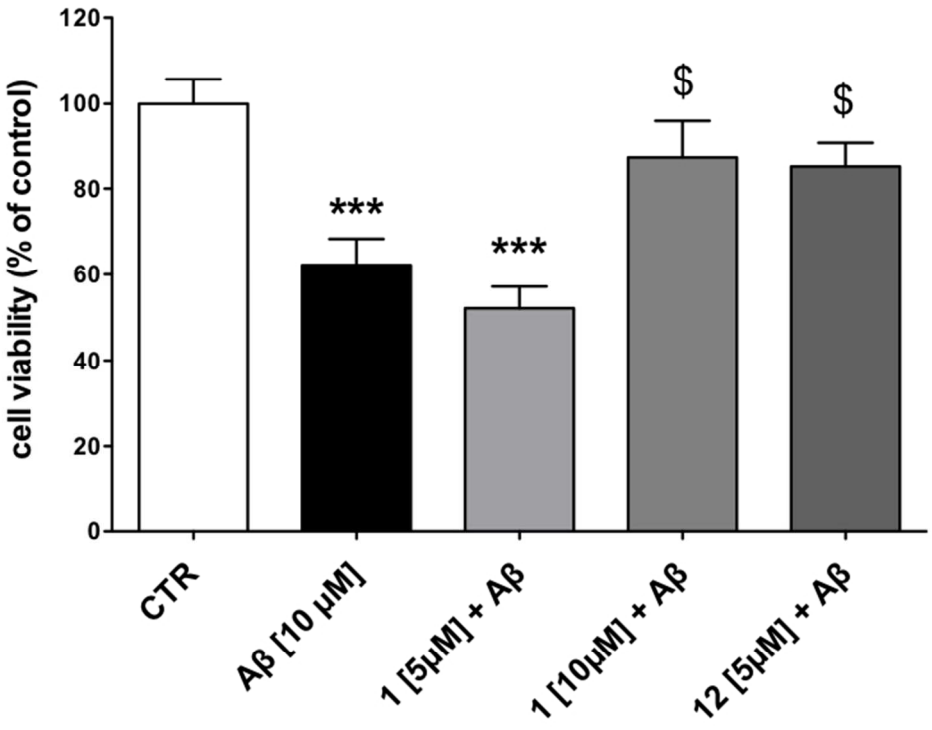

Figure 3. Effect of 1 and 12 on Aβ42-mediated toxicity in neuroblastoma cells. SH-SY5Y cells were co-incubated for 24 h with 5 μM and 10 μM compound 1 or with 5 μM compound 12 in presence of 10 μM Aβ42. Cell viability was determined by MTT assay. Data are expressed as percentage of cell viability versus CTR; ***p<0.001 versus CTR, $ p<0.05 versus Aβ42; Dunnett's multiple comparison test.

66x50mm (300 x 300 DPI)

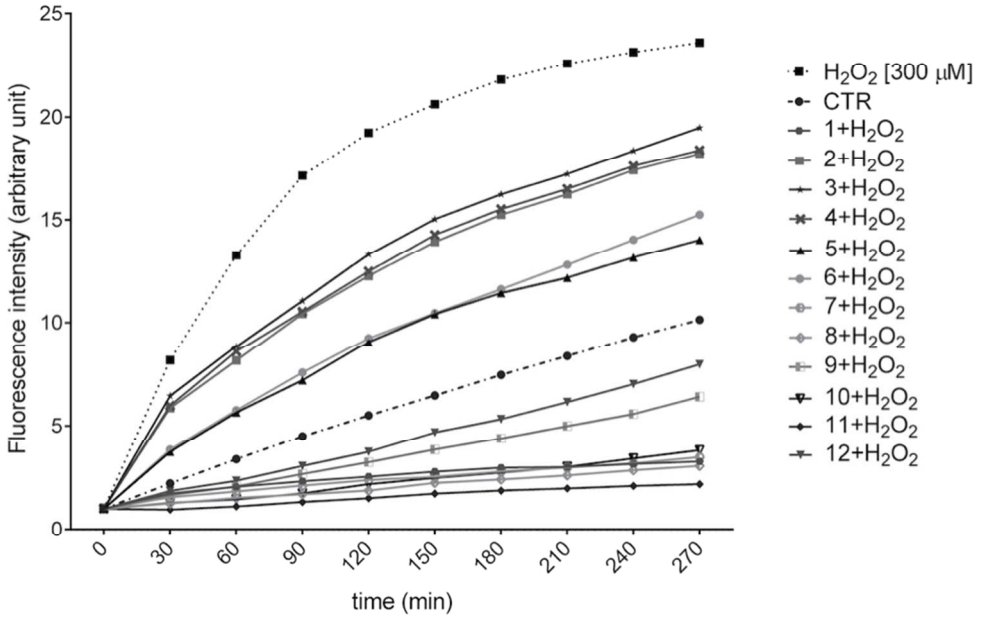

Figure 4. Compounds 1-12 reverse ROS formation induced by H_2O_2-induced oxidative stress in SH-SY5Y neuroblastoma cells. Cells were loaded with 25 mM DCFH-DA for 45 min. DCFH-DA was removed by centrifugation, cells were resuspended in PBS into a black 96-wells plate and exposed to 5 μM concentration of compounds 1-12 and 300 μM H_2O_2. ROS levels were determined from 0 to 270 min using a fluorescence microplate reader. Fluorescence intensity for all compounds is significant at any time from 30 to 270 min with $p<0.001$ versus H_2O_2. Dunnett's multiple comparison test.

84x55mm (300 x 300 DPI)

a

Total Nrf2 protein expression levels										
	CTR	1	5	7	8	9	10	11	12	13
Nrf2/ tubulin	100,0	411,3	339,9	383,1	188,0	372,3	198,7	231,5	367,3	138,7
SEM	7,835	42,60	43,64	28,51	21,18	58,03	28,04	15,89	63,32	14,44
P-value	/	< 0,0001	< 0,0001	< 0,0001	0,5640	0,0002	0,4378	0,1617	< 0,0001	0,9813

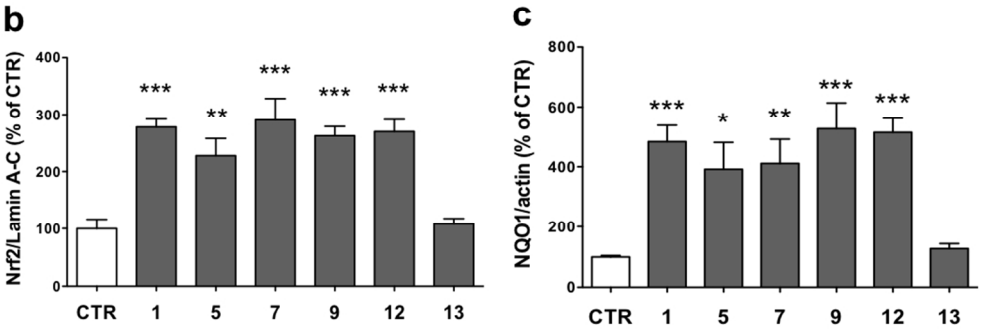

Figure 5. Activation of Nrf2-mediated phase II detoxification pathway. a) Total cellular extracts of SH-SY5Y cells treated for 24 h with 5 μM concentration of compounds 1, 5, 7-13 were analyzed for Nrf2 expression by western blot. Anti tubulin was used as protein loading control. Results are shown as ratio Nrf2/tubulin (% of CTR) ± SEM. Dunnett's multiple comparison test. b) Nuclear cellular extracts of SH-SY5Y cells were treated for 3 h with compounds 1, 5, 7, 9, 12, 13 at 5 μM concentration and homogenized to obtain nuclear fraction. Nrf2 expression was determined by western blot. Anti lamin A-C was used as protein loading control. Results are shown as ratio Nrf2/lamin A-C (% of CTR) ± SEM. **p<0.01 and ***p<0.001 versus CTR; Dunnett's multiple comparison test. c) Total cellular extracts of SH-SY5Y cells treated for 24 h with 5 μM concentration of compounds 1, 5, 7, 9, 12, 13 were analyzed for NQO1 expression by western blot. Anti-actin was used as protein loading control. Results are shown as ratio NQO1/actin (% of CTR) ± SEM. *p<0.05, **p<0.01 and ***p<0.001 versus CTR; Dunnett's multiple comparison test.

90x57mm (300 x 300 DPI)

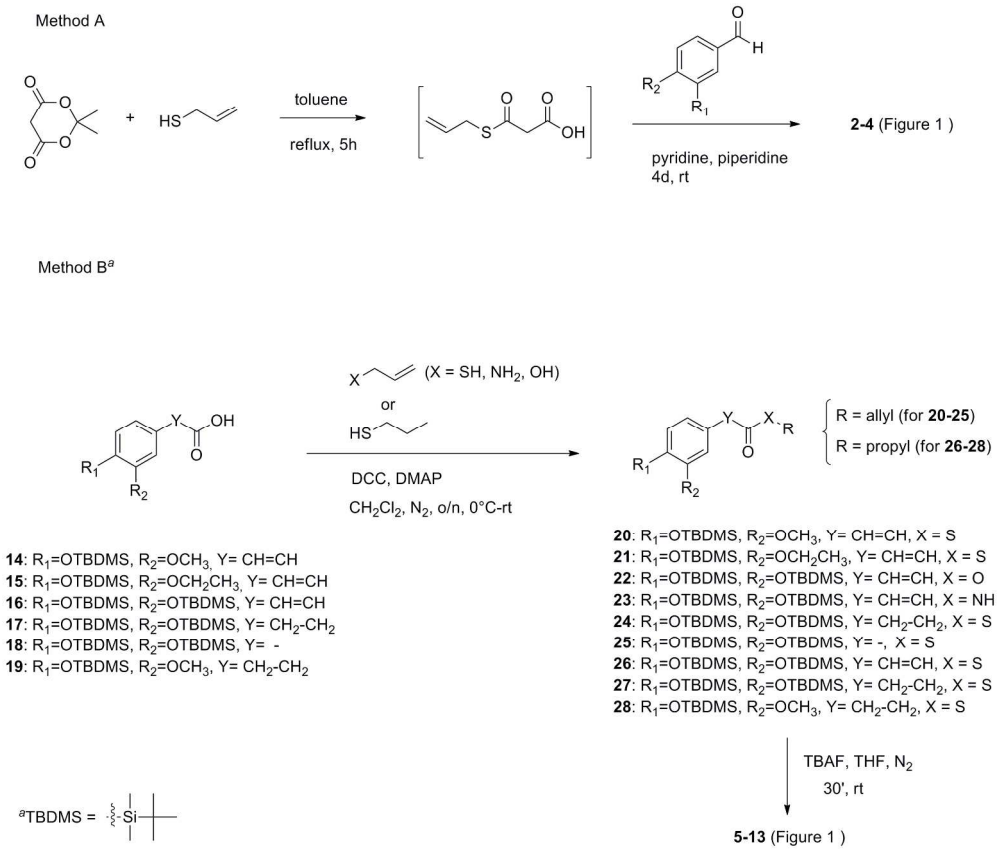

217x183mm (300 x 300 DPI)

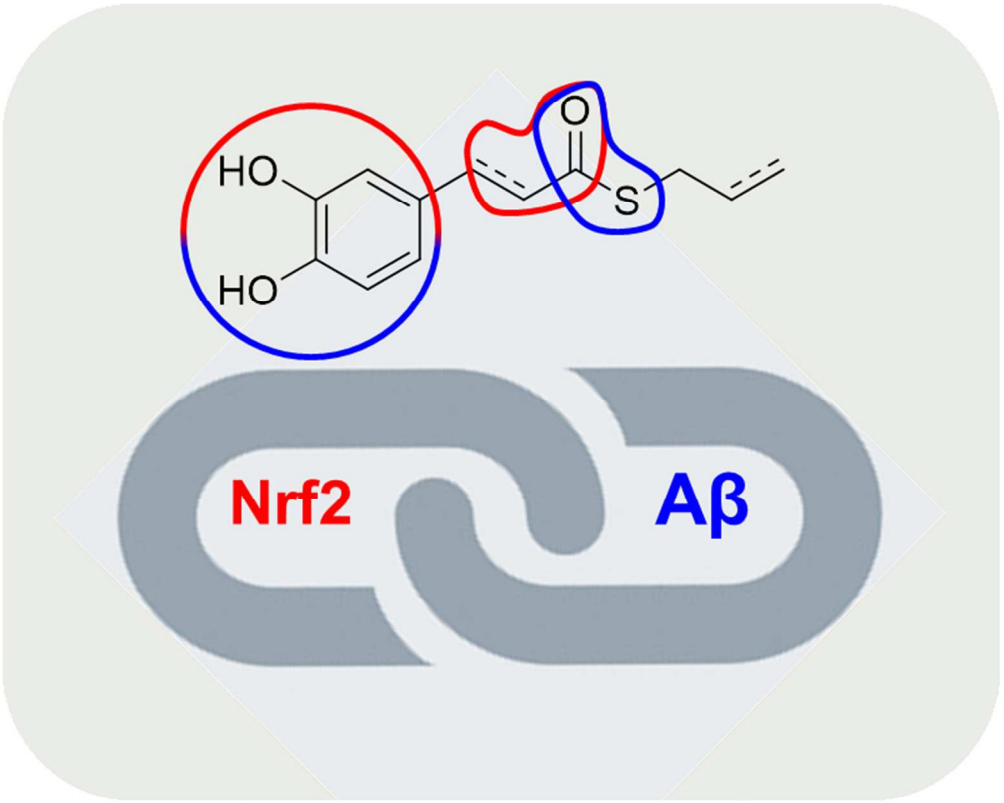

Graphical Table of Contents

67x66mm (300 x 300 DPI)